Bull Volcanol (2005) 68: 135–156
DOI 10.1007/s00445-005-0428-4

RESEARCH ARTICLE

Ingrid Ukstins Peate · Joel A. Baker · Mohamed Al-Kadasi · Abdulkarim Al-Subbary · Kim B. Knight · Peter Riisager · Matthew F. Thirlwall · David W. Peate · Paul R. Renne · Martin A. Menzies

Volcanic stratigraphy of large-volume silicic pyroclastic eruptions during Oligocene Afro-Arabian flood volcanism in Yemen

Received: 18 August 2003 / Accepted: 14 March 2005 / Published online: 6 October 2005

Abstract A new stratigraphy for bimodal Oligocene flood volcanism that forms the volcanic plateau of northern Yemen is presented based on detailed field observations, petrography and geochemical correlations. The >1 km thick volcanic pile is divided into three phases of volcanism: a main basaltic stage (31 to 29.7 Ma), a main silicic stage (29.7 to 29.5 Ma), and a stage of upper bimodal volcanism (29.5 to 27.7 Ma). Eight large-volume silicic pyroclastic eruptive units are traceable throughout northern Yemen, and some units can be correlated with silicic eruptive units in the Ethiopian Traps and to tephra layers in the Indian Ocean. The silicic units comprise pyroclastic density current and fall deposits and a caldera-collapse breccia, and they display textures that unequivocally identify them as primary pyroclastic deposits: basal vitrophyres, eutaxitic fabrics, glass shards, vitroclastic ash matrices and accretionary lapilli. Individual pyroclastic eruptions have preserved on-land volumes of up to ~850 km^3. The largest units have associated co-ignimbrite plume ash fall deposits with dispersal areas $>1\times10^7$ km^2 and estimated maximum total volumes of up to 5,000 km^3, which provide accurate and precisely dated marker horizons that can be used to link litho-, bio- and magnetostratigraphy studies. There is a marked change in eruption style of silicic units with time, from initial large-volume explosive pyroclastic eruptions producing ignimbrites and near-globally distributed tuffs, to smaller volume (<50 km^3) mixed effusive-explosive eruptions emplacing silicic lavas intercalated with tuffs and ignimbrites. Although eruption volumes decrease by an order of magnitude from the first stage to the last, eruption intervals within each phase remain broadly similar. These changes may reflect the initiation of continental rifting and the transition from pre-break-up thick, stable crust supporting large-volume magma chambers, to syn-rift actively thinning crust hosting small-volume magma chambers.

Keywords Continental flood volcanism · Volcanic stratigraphy · Yemen · Ethiopia · Bimodal volcanism · Ignimbrite · Rhyolite · Flood basalt

Electronic Supplementary Material Supplementary material is available for this article at http://dx.doi.org/10.1007/s00445-005-0428-4

I. U. Peate (✉) · D. W. Peate
Department of Geoscience, University of Iowa,
121 Trowbridge Hall, Iowa City, IA 52242 USA
e-mail: ingrid-peate@uiowa.edu
Tel.: +319-335-1824
Fax: +319-335-1821

I. U. Peate · M. F. Thirlwall · M. A. Menzies
Department of Geology, Royal Holloway University of London,
Egham, Surrey, TW20 OEX, England

J. A. Baker
School of Earth Sciences, Victoria University of Wellington,
P.O. Box 600, Wellington, New Zealand

M. Al-Kadasi · A. Al-Subbary
Department of Geology, Faculty of Science, Sana'a University,
P.O. Box 1247, Sana'a, Yemen

K. B. Knight · P. R. Renne
Department of Earth and Planetary Science, University of California,
Berkeley, CA 94709, USA

K. B. Knight · P. R. Renne
Berkeley Geochronology Center,
2455 Ridge Road, Berkeley, CA 94709, USA

P. Riisager
Department of Geology, Lund University,
Sölvegata 12,
S-223 62 Lund, Sweden

Introduction

Establishing a well-constrained volcanic stratigraphy is crucial for understanding the evolution of flood volcanic provinces and their relationship to continental rifting and break-up. It is an often neglected aspect of continental flood volcanic province studies, but one that underpins the framework of sampling for both geochemical and

geochronological studies (e.g. Mangan et al. 1986; Beane et al. 1986; Peate et al. 1990, 1992; Jerram 2002; Ukstins Peate et al. 2003a). Large volume silicic units in some large igneous provinces can form important, laterally continuous, distinctive marker horizons that constrain the volcanic stratigraphy over several hundred km in an otherwise often monotonous and internally complex flood basalt lava succession. In extreme cases, individual silicic eruptive units can span a large part of the areal extent of the flood volcanic province, such as in the Paraná-Etendeka (e.g. Milner et al. 1992, 1995; Ewart et al. 1998). In addition, descriptions of the volcanological features of the silicic units associated with flood basalt provinces are sparse in the literature (with the notable exception of the Paraná-Etendeka province: e.g. Milner et al. 1992; Bryan et al. 2002), and yet these provide important information about eruption processes between different provinces.

In this paper, we present a detailed volcanic stratigraphy for the portion of the Oligocene Afro-Arabian continental flood volcanic province preserved in northern Yemen. We focused on this region rather than the volumetrically larger part of the province in Ethiopia because of the excellent exposure and the limited tectonic disruption of stratigraphic sections from post-break-up processes in Yemen. The stratigraphy was constructed using field and petrographic observations, together with new compositional data, and integrated with published compositional and geochronological data from both Yemen and Ethiopia (Baker et al. 1996a, 1996b; Hofmann et al. 1997; Ayalew et al. 2002; Ukstins et al. 2002), as well as new $^{40}Ar/^{39}Ar$ data (Riisager et al. in press). We also present detailed descriptions of the physical volcanology of well-preserved large-volume silicic pyroclastic rocks. These new stratigraphic, chronological and volcanological observations allow us to characterize the rates, volumes, and mechanisms of eruptions, as well as temporal variations in these characteristics during Afro-Arabian continental break-up and the transition to syn-rift volcanism in Yemen.

Geological setting

The extensive Ethiopian traps in Africa and the volcanic plateau in Yemen originally formed a single magmatic province (Fig. 1: Mohr 1983; Mohr and Zanettin 1988) that was closely associated with the opening of the Red Sea and Gulf of Aden during the early Oligocene (31 to 26 Ma: e.g. Davidson and Rex 1980; Baker et al. 1996a; Hofmann et al. 1997; Rochette et al. 1998; Ukstins et al. 2002). The distribution of Afro-Arabian flood volcanism on the conjugate rift margins of the Red Sea and Gulf of Aden is highly asymmetrical (Fig. 1), with ~90% preserved on the African plate in Ethiopia, Djibouti and Eritrea (>350,000 km^3). The earliest volcanism in both Yemen and Ethiopia was emplaced onto a regional lateritic paleosol horizon, perhaps produced by progressive sediment starvation in response to topographic changes related to the initiation of volcanism (McDougall et al. 1975; Davidson and Rex 1980; Berhe et al. 1987; WoldeGabriel et al. 1990; Davison et al. 1994; Drury et al. 1994; Al-Subbary 1995). In Yemen, there is evidence for significant uplift (10's of m: Al-Subbary 1995) from a shallow marine depositional environment to fluvial continental clastic deposition immediately preceding volcanism.

The Afro-Arabian flood volcanic succession is composed of basaltic lavas, rhyolitic ignimbrites and pyroclastic fall deposits, in addition to less common basaltic pyroclastic rocks and rhyolitic lavas (e.g. Civetta et al. 1978; Mohr 1983; Capaldi et al. 1983; Chiesa et al. 1983; Berhe et al. 1987; Mohr and Zanettin 1988; Manetti et al. 1991; Baker et al. 1996a, 1996b; Pik et al. 1998; Ayalew et al. 2002; Ukstins et al. 2002). While a generalized volcanic stratigraphy does exist for the Ethiopian part of the province (Mohr 1983; Mohr and Zanettin 1988), no regionally applicable, detailed stratigraphic model has been established there due to the poor exposure that results from extensive faulting, continuing syn-rift volcanism and a climate that has produced extensive vegetation covering outcrops (Ukstins et al. 2002). In contrast, the Yemen plateau is relatively untectonized, and it has excellent exposure due to the arid environment, enhanced by post-break-up uplift and erosion that have dissected and exposed the flood volcanic succession (Baker 1996; Baker et al. 1996a, b; Menzies et al. 1997).

Field and analytical methods

Field work was carried out in 1999 in the Sana'a area of northern Yemen and the volcanic plateau escarpment to the west (an area of ~10,000 km^2: Fig. 1). A series of ten stratigraphic sections, which range in thickness from ~50 m to >1 km, were logged and sampled (Fig. 2). All sections were also sampled for paleomagnetic studies during these field investigations (Riisager et al. 2001). Two sections rest on Cretaceous-Paleogene pre-volcanic sandstones, and thus provide constraints on the timing of the local initiation of flood volcanism. There are variable amounts of stratigraphic overlap among the sections, and this allows us to examine lateral changes in unit thickness and morphology. The sections provided a large and stratigraphically well-constrained sample suite covering all major volcanic units (silicic ash flow and air fall deposits, and silicic and basaltic lavas, including additional data from Baker 1996, see online appendix of stratigraphic sections). These samples were analyzed for major and trace element concentrations by X-ray fluorescence spectrometry and a subset of samples for rare earth elements by isotope dilution mass spectrometry (Baker et al. 2002) (analytical details are given in the appendix, and the full data set are provided in the online data set). In addition, the Pb isotope compositions of the silicic samples were measured by in situ laser ablation multi-collector ICP-MS on the groundmass of rock chips and also on selected whole rock samples by Pb double-spike methods (Baker et al. 2004) (full data set is presented in Ukstins Peate et al. 2003b). Nd isotope compositions of a representative sample of each of the stratigraphically prominent units are also given in Table 3.

$^{40}Ar/^{39}Ar$ ages on a suite of 12 stratigraphically important mafic and silicic units were determined at the Berkeley Geochronology Center. Full details of these new ages will be presented in a forthcoming manuscript (Riisager et al., in press) describing the paleomagnetic results and tying them into the magnetic chron timescale. Pertinent $^{40}Ar/^{39}Ar$ ages including those already published by Baker et al. (1996a) and Ukstins et al. (2002), and paleomagnetic polarities are annotated on Fig. 2, and summarized in Table 1 for each of the stratigraphically prominent units. All $^{40}Ar/^{39}Ar$ ages are reported with 2σ errors, relative to Fish Canyon sanidine with an age of 28.02 Ma (Renne et al. 1998).

Volcanic stratigraphy of the northern Yemen plateau

Methodology and overview

An initial volcanic stratigraphy was constructed from field observations and logged sections, and refined by chemostratigraphic correlations (Fig. 2). Variations in textural characteristics, petrography and paleomagnetic polarity provide additional constraints on the stratigraphy. Of the geochemical correlation parameters, Pb isotope ratios proved to be the most useful for distinguishing individual silicic eruptive units, as most units fall into two main groups, a "high $^{208}Pb/^{206}Pb$" and a "low $^{208}Pb/^{206}Pb$" group (see Ukstins Peate et al. 2003b). By utilizing an extensive database of in situ Pb isotope analyses (Ukstins Peate et al. 2003b), in conjunction with major and trace element concentrations, we establish compositional correlations among units that corroborate and expand the stratigraphy established by field observations. While two units exhibit major and trace element compositional zonations, Pb and Nd isotopic ratios are constant and extremely useful for establishing chemostratigraphic correlations (with the notable exception of the chemically and isotopically zoned Sam Ignimbrite, discussed in detail below). Analysis of pumice clast separates provides the most reliable indicator of the true magma composition and reduces problems of mechanical sorting of pyroclastic deposits during magma fragmentation and transport (Wolff 1985). However, most ignimbrites

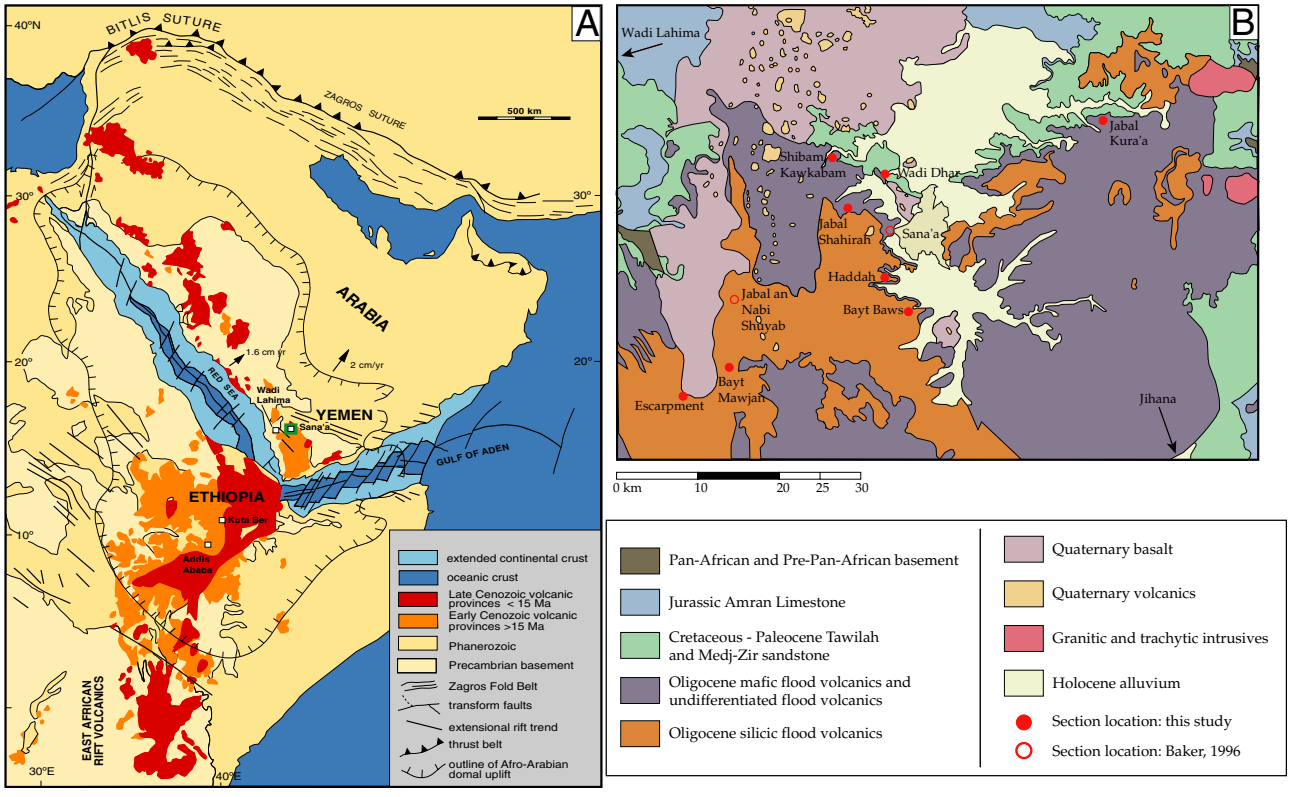

Fig. 1 **A**. Distribution of Cenozoic volcanism in the Red Sea and Gulf of Aden region (modified after Davison et al. 1994; Baker et al. 1996a). Continental magmatism is divided into two groups; an older group (>15 Ma) of bimodal mafic and silicic flood volcanics that are the focus of this paper, and a younger group of predominantly alkaline mafic synrift volcanics. Yemen is located at the southwestern tip of the Arabian peninsula, and prior to the formation of the Red Sea-Gulf of Aden oceanic rifts, Yemen was juxtaposed against Ethiopia and Eritrea. The onshore flood volcanic samples come from field areas in Yemen and Ethiopia, which are marked by *square boxes*. The Kuta Ber section, which has exposures of Oligocene flood volcanic rocks described in detail by Ukstins et al. (2003b), is located on the northern escarpment in the Ethiopian field area. The Wadi Lahima section, discussed in the text, is located in western Yemen. The Sana'a area of Yemen is marked with a *green box* and is illustrated in detail in the geological map presented in Fig. 1B. **B**. Geological map of the Sana'a area, Yemen, modified after Kruck (1983). Locations of the ten sampled sections from this study are shown, and sections are divided into those from Baker (1996) and Ukstins Peate (2003). The Sana'a and Jabal Shahirah sections and the Jabal an Nabi Shuyab and Bayt Mawjan sections cover equivalent stratigraphic intervals. Quaternary volcanics are undifferentiated mafic to intermediate units. Detailed stratigraphic sections for eight sampled profiles are shown in Fig. 2

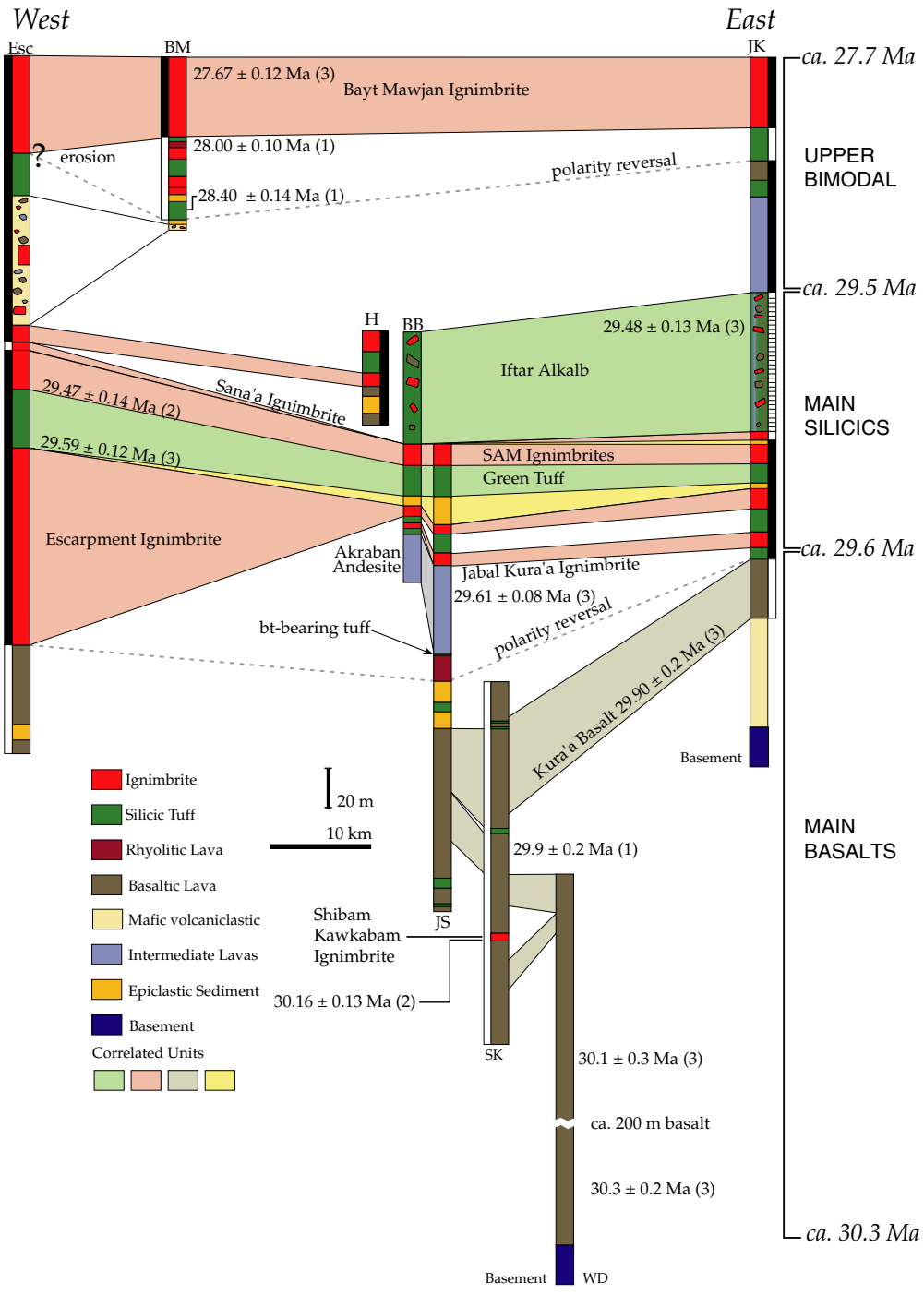

Fig. 2 Schematic volcanic stratigraphy of flood volcanic units emplaced during Oligocene bimodal volcanism in northern Yemen. All stratigraphic sections are relative to the same vertical scale and have been arranged to reflect spatial (E–W) distances as well as elevation differences between sections (see Fig. 1B for location information). Section abbreviations, from east to west, are: JK: Jabal Kura'a, WD: Wadi Dhar, SK: Shibam Kawkabam, JS: Jabal Shahirah, BB: Bayt Baws, H: Haddah, BM: Bayt Mawjan, Esc: Escarpment. Jabal Kura'a, Shibam Kawkabam, Haddah, Bayt Mawjan and Escarpment sections are annotated with paleomagnetic polarity data (white = reverse, black = normal) after Riisager et al. (2001) and Riisager et al. (in press). Iftar Alkalb mega-breccia is illustrated as a column colored to reflect the dominant composition of the matrix material with clasts representing the mafic and silicic units included within. The mafic breccia in the Escarpment section also reflects the matrix and clast compositions. The Wadi Dhar section contains an additional 200 m of reversely magnetized basaltic lavas that are not shown in detail here, but are differentiated in the online stratigraphic appendix, and overlies sedimentary basement (Tawilah Group) found at the base of the section. The Jabal Kura'a section also contacts basement at the base of the section. Ages are $^{40}Ar/^{39}Ar$ dates from (1) Baker et al. (1996a), (2) Ukstins et al. (2002) and (3) data presented here and in Riisager et al. (in press)

Table 1 Summary of field and petrographic features for main units, Oligocene flood volcanism, Yemen

Unit (youngest to oldest)	Age (Ma)	Polarity	Stratigraphic group	Sections[a]	Thickness	Unit type	Comments	Modal mineralogy				
								Fsp	Cpx	Fe-Ti	Amp	Qtz
Bayt Mawjan Ignimbrite	27.67 ± 0.12 (3)	N	Upper Bimodal	JK, BM, ESC	35 to 50 m (thickens towards W)	Ignimbrite	Welded, basal vitrophyre	√	√	√		√
Bimodal volcanics	29.5 to 27.7	M	Upper Bimodal	JK, BM	5 tuffs, 3 igs, 1 rhyolite, basaltic lavas	Ash fall and flow, basaltic & silicic lavas	Thin units, hydrous mineralogy	√	√	√	√	√
Upper Series Basalts (after Baker et al. (1996b))	<29.5	?	Upper Bimodal	BM, ESC, Sana'a area	~100 m basaltic lavas	Basaltic lavas, mafic breccia	Intercalated with main silicic units	√	√	√		
Iftar Alkalb	29.48 ± 0.13 (3)	N	Main Silicic	JK, BB	70 to 150 m	Caldera collapse breccia	Mega-breccia, rheomorphic folds	√	√	√		
Sana'a Ignimbrite	~29.5	R	Main Silicic	JK, ESC	~5 m	Ignimbrite	Negative polarity	√	√	√		
Sam Upper Ignimbrite	29.47 ± 0.14 (2)	N	Main Silicic	JK, JS, BB, ESC, ETH	5 to 10 m (thickens towards W)	Ignimbrite	Welded	√	√	√		
Sam Lower Ignimbrite	29.47 ± 0.14 (2)	N	Main Silicic	JK, JS, BB, ESC, ETH, IO	7 to 15 m (thickens towards W)	Ignimbrite	Welded	√	√	√		
Green Tuff	29.59 ± 0.12 (3)	N	Main Silicic	JK, JS, BB, ESC	10 to 20 m (thickens towards W)	Ash fall	Cuspate ash shards	√	√	√		
Escarpment Ignimbrite	~29.6	N	Main Silicic	JK, JS, BB, ESC	5 to >100 m (thickens towards W)	Ignimbrite	Rheomorphic, basal vitrophyre	√	√	√		√
Jabal Kura'a Ignimbrite	~29.6	N	Main Silicic	JK, JS, BB, IO	5 to 9 m	Ignimbrite	Nonwelded, lithics	√	√	√		√
Akraban Andesite	29.61 ± 0.08 (3)	N	Main Basalt	JS, BB	50 m	Lava flow		√				
Fine-grained tuffs above SK lg	~30.1 to 29.9	R	Main Basalt	SK, JS	0.5 to 5 m	Ash fall and epiclastic	Altered					
Shibam Kawkabam Ignimbrite	30.16 ± 0.13 (2)	R	Main Basalt	SK, ETH	Unknown (15 m in Ethiopia)	Ignimbrite	Nonwelded, mafic scoria	√	√	√		

Ages quoted for individual units are $^{40}Ar/^{39}Ar$ ages from: (1) Baker et al. (1996a), (2) Ukstins et al. (2002) and (3) Riisager et al. (in press). Estimated ages and age ranges are based on the aforementioned $^{40}Ar/^{39}Ar$ age sources and the volcanic stratigraphy compiled here (Fig. 2). Paleomagnetic polarity (Pol) is delineated as normal = N, reverse = R, and M = mixed after Riisager et al. (2001) and Riisager et al. (in press). Stratigraphic sections are presented in Fig. 2 and abbreviations are: JK = Jabal Kura'a, SK = Shibam Kawkabam, JS = Jabal Shahirah, BB = Bayt Baws, H = Haddah, BM = Bayt Mawjan, Esc = Escarpment, ETH = Ethiopia, and IO = Indian Ocean. Modal mineralogy abbreviations are: fsp = feldspar (dominantly potassium feldspar), cpx = clinopyroxene, Fe-Ti – iron-titanium oxide minerals, amp = amphibole, and qtz = quartz

[a]See Fig. 2

and tuffs from this study were devoid of pumice clasts, or lithified and/or welded, as well as generally being lithic and crystal-poor, so only whole-rock sample analysis was possible. Samples were handpicked from coarse-crushed chips to exclude any apparent xenoliths (see Appendix 1: analytical methods).

Figure 3 illustrates the distribution of ~250 mafic and silicic samples on a TAS diagram (after Le Bas et al. 1986; data from Baker 1996 and Ukstins Peate 2003, see also online dataset), and shows a prominent silica gap between 55 and 67 wt.% SiO_2. Intermediate compositions represented by units such as the Akraban Andesite are few and limited in extent. It is important to emphasize that the underlying causes for the major compositional changes between units (e.g. source heterogeneity, partial melting differences, extent of magma differentiation or crustal assimilation) are not the immediate concern in developing a volcanic stratigraphy, although the recognition of distinct magma types can eventually lead to improvements in the understanding of the complex petrogenetic history of the province as a whole (e.g. Peate et al. 1992). While the breadth of this paper does not encompass the petrogenetic history of the silicic units discussed here, this is an important issue and will be addressed in a separate paper.

Correlated units exhibit consistent stratigraphic and age relationships across the northern Yemen plateau (Fig. 2), and are characterized by their distinctive field appearance, petrography, major and trace element compositions, and Pb-Nd isotope ratios. Textural characteristics, $^{40}Ar/^{39}Ar$ age data, petrographic and mineralogical descriptions, and distinctive geochemical features for the main eruptive units are summarized in Table 1. Average geochemical analyses for each of the silicic eruptive units are presented in Tables 2, and 3 summarizes the main and distinguishing geochemical features of the silicic eruptive units.

These new stratigraphic data allow the Afro-Arabian volcanic evolution of the Sana'a area of the northern Yemen plateau to be divided into three phases: (from oldest to youngest, Fig. 2): (1) *a main flood basalt phase* (~30.3 to 29.7 Ma), (2) *a main silicic pyroclastic phase* (29.7 to 29.5 Ma), and (3) *an upper bimodal volcanic phase* (29.5 to 27.7 Ma). The discussion below will present each of the three main phases of volcanism with an overview, followed by detailed descriptions of the principle stratigraphic units within each phase. Additionally, ages for each phase of volcanism and for specific units, as well as latitude and longitude measurements for the type localities of specific principle units are given in the subheadings below.

Main flood basalt phase (~30.3 to 29.7 Ma)

The initiation of volcanism, the *main flood basalt phase*, is characterized by dominantly effusive emplacement of voluminous flood basalt lava flows. Also found intercalated with the lavas are minor basaltic pyroclastic rocks, usually located near the base of the lava succession (Ross et al. 2005), epiclastic deposits which include reworked fine-grained silicic airfall tuffs, rare intermediate and sili-

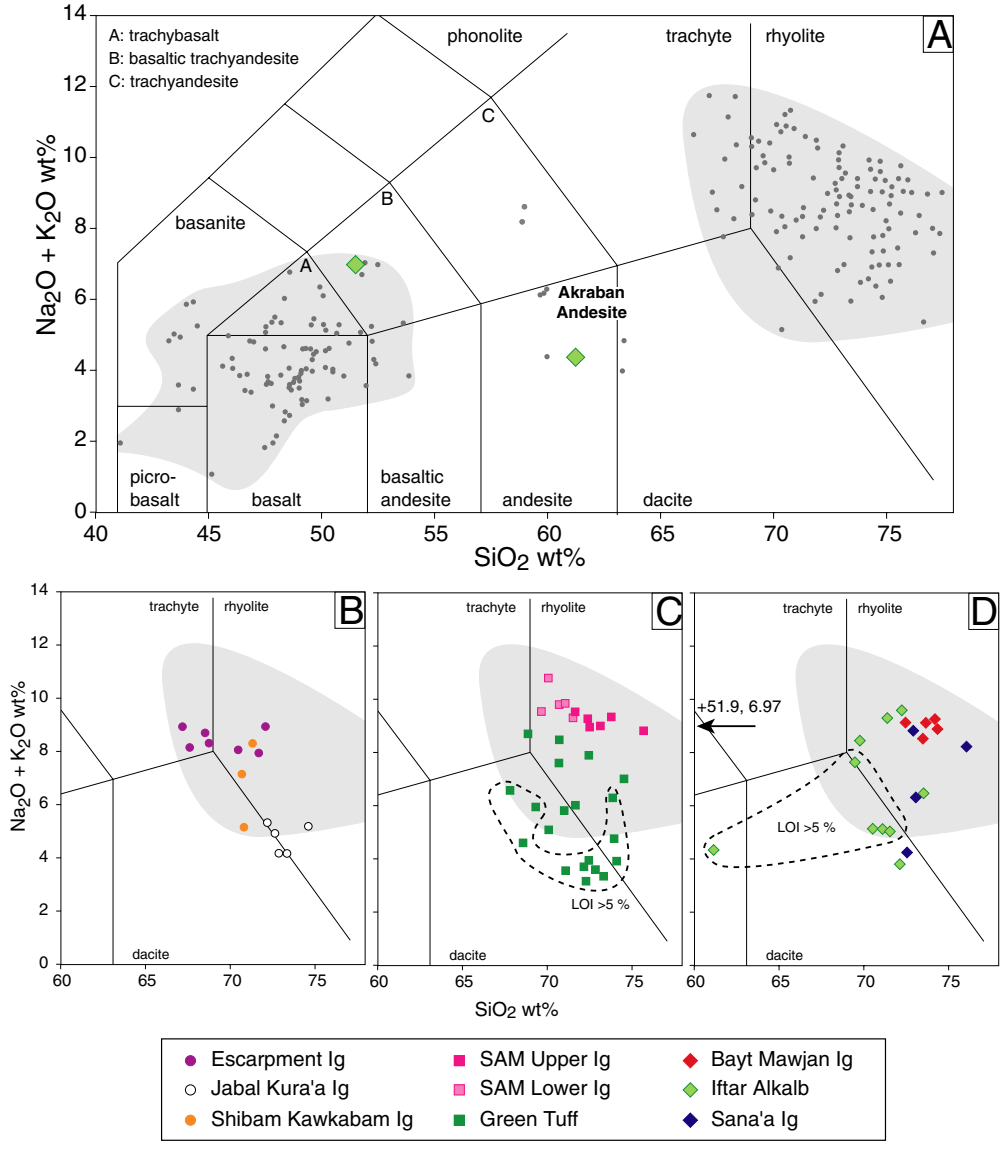

Fig. 3 **A**. Total alkalis – silica classification diagram after Le Bas et al. (1986) showing the bimodal distribution of Afro-Arabian Oligocene flood volcanic rocks (*light gray fields*) with individual analyses from Yemen shown as *dark gray circles*. Two analyses of Iftar Alkalb with intermediate to mafic compositions are plotted here also. **B**–**D**. An abbreviated version of the TAS diagram showing intermediate to silicic compositions with individual analyses for nine main silicic units from Yemen plotted as individual *circles*, *squares* and *diamonds*. Jabal Kura'a and Shibam Kawkabam Ignimbrites have an additional sample plotted on Fig. 3 that has been eliminated from the following diagrams (Figs. 5 and 6) due to high LOI values (see supplementary data). The Green Tuff and Iftar Alkalb have significant numbers of samples with LOI >5%, and these samples have been outlined with *dashed lines* on C and D

cic lava flows, and a single ignimbrite deposit (the Shibam Kawkabam ignimbrite) (Fig. 2). This phase is the volumetrically dominant component of volcanism, representing 60 to 70% of the total erupted volume, with average eruption intervals of 10 to 100 kyr per flow (Baker et al. 1996a), and estimated single-flow volumes of ~10 km^3. The mafic rocks comprise a variety of lava compositions, primarily basalts and trachybasalts (>75%) with some picro-basalts, basaltic andesites, basaltic trachyandesites, and rare andesite flows (Fig. 3). The basalts are variably olivine + clinopyroxene phyric and more evolved lavas also contain phenocrysts of plagioclase ± Fe-Ti oxides (Baker et al. 2000).

Significant lateral variations occur in the basal basaltic volcanic succession. In the Sana'a area, sections range from ~50 m of mafic volcaniclastic deposits (including both epiclastic sediments and basaltic pyroclastic deposits of tuff containing accretionary lapilli: Ross et al. 2005) in the Jabal Kura'a section, to a >250 m thick sequence of ponded lava flows at Wadi Dhar, where some lava flow units have individual thicknesses up to 50 m (Fig. 2). Some basaltic lava flows can be geochemically correlated between sections in the Sana'a area (Jabal Shahirah, Shibam Kawkabam, Wadi Dhar sections: Fig. 2). To the west, in the Escarpment section, the lowest exposed flows underlying the first ignimbrite in that section (Fig. 2) are petrographically dis-

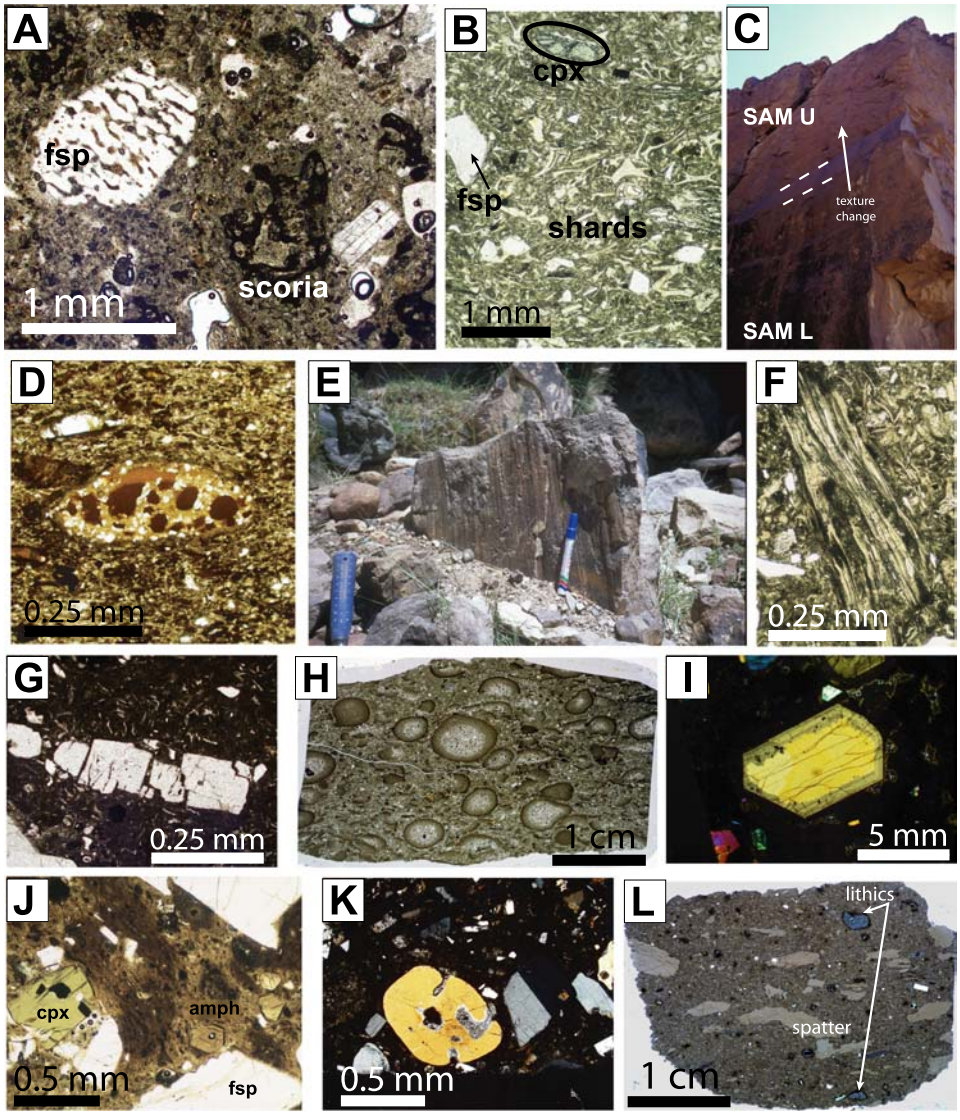

Fig. 4 **A**. Thin section photomicrograph of the Shibam Kawkabam Ignimbrite from the Shibam Kawkabam section (YIU99001), showing a vesicular scoriaceous bleb (*lower right*) and a sieve-textured feldspar phenocryst (*upper left*). Scoriaceous clasts compose a small volume percentage of the deposit (less than 5%) and would not contribute significantly to the major element composition of the unit as a whole. **B**. Thin section photomicrograph of the Green Tuff from the Jabal Shahirah section (JB276, Baker 1996 and online stratigraphy appendix), showing feldspar and clinopyroxene phenocrysts, in a well-defined tricuspate glass shard matrix. **C**. Field photograph of the Sam Ignimbrite from the Jabal Kura'a section showing the contact between the Sam L and Sam U Ignimbrite units. The fine-grained layer in the center of the photograph (delineated with *dashed lines*), may represent the basal layer of the upper Sam Ignimbrite, although there are no obvious stratigraphic breaks or geochemical changes from the top of Sam L to this fine-grained layer to the overlying platy-jointed layer representing Sam U. **D**. Thin section photomicrograph of a sample from near the top of the Sam U Ignimbrite (YIU99098) in the Bayt Baws section (Fig. 2 and online stratigraphy appendix). Glassy brown blebs are common, The largest one, shown here, is partly devitrified and altered in a streaky texture. **E**. Field photograph from the Jabal Kura'a section that shows a block of Sam Ignimbrite in Iftar Alkalb with slickensides, which may represent slickenlines formed within a moving pyroclastic unit (Calder et al. 2000). Marker pen for scale is 15 cm. **F**. Thin section photomicrograph showing pumice in Iftar Alkalb, Jabal Kura'a section (JB214). **G**. Photomicrograph of a thin section from YIU99172, sampled near the top of the Iftar Alkalb exposure in the Jabal Kura'a section, showing a shattered "jigsaw phenoclast" of feldspar in a fine grained matrix with visible ash shards. **H**. Thin section photograph from Iftar Alkalb mega-breccia (YIU99130, Ukstins Peate 2003), sampled near the bottom third of the Iftar Alkalb exposure in the Jabal Kura'a section, showing an extremely well preserved accretionary lapilli horizon with whole, weakly compacted lapilli and broken lapilli in an ash matrix. **I**. Photomicrograph of a thin section from sample YIU99185, a basaltic clast from the breccia at the base of the Bayt Mawjan section, correlated with the breccia found in the Escarpment section, photographed with crossed polarizing filters. The euhedral clinopyroxene crystal exhibits a core with resorbed edges and complexly zoned overgrowth. **J**. Thin section photomicrograph of a unit from the upper bimodal phase in the Bayt Mawjan section (YIU99193, Ukstins Peate 2003), showing amphibole, clinopyroxene and potassium feldspar phenocrysts in an opaques and ash-rich matrix. **K**. Thin section photomicrograph of a unit from the upper bimodal phase in the uppermost Jabal Kura'a section (YIU99121), showing a rounded and embayed quartz phenocryst with a microcrystalline silicic melt in the embayments. **L**. Thin section photograph, of the basal vitrophyre of the Bayt Mawjan Ignimbrite in the Bayt Mawjan section (YIU99195, Ukstins Peate 2003). Attenuated glassy juvenile spatter clasts occur in a welded glassy matrix. Phenocrysts of feldspar and quartz, and gray lithic clasts are also present

Table 2 Average major and trace element compositions for main silicic pyroclastic units, Oligocene flood volcanism, Yemen

Unit	SK Ig	2 sd	Akraban	2 sd	JK Ig	2 sd	Esc Ig	2 sd	G Tuff	2 sd	Sam-L	2 sd	Sam-U	2 sd	Sana'a	2 sd	IA	2 sd	BM Ig	2 sd
wt.%	*n*=2	sect=1	*n*=2	sect=2	*n*=4	sect=2	*n*=7	sect=4	*n*=8	sect=4	*n*=6	sect=4	*n*=5	sect=2	*n*=3	sect=2	*n*=5	sect=2	*n*=8	sect=4
SiO_2	71.12	0.47	59.97	0.06	71.94	2.07	69.72	1.84	71.79	1.81	71.62	0.94	73.48	1.60	74.62	1.67	67.97	9.11	73.73	1.44
Al_2O_3	12.48	0.24	13.02	0.01	12.92	0.45	13.55	1.03	13.56	1.02	12.86	0.55	11.93	0.53	12.33	1.12	13.93	1.13	12.79	0.57
Fe_2O_3	4.21	0.05	13.27	0.01	3.72	1.28	6.02	1.17	3.94	1.61	3.35	0.37	3.31	0.26	3.20	0.25	5.09	4.27	2.76	0.43
MgO	2.21	0.23	0.91	0.00	0.67	0.46	0.47	0.22	0.75	0.22	0.44	0.21	0.32	0.11	0.42	0.43	1.25	1.10	0.22	0.16
CaO	1.04	0.58	4.64	0.01	1.20	0.85	1.14	0.47	1.68	0.93	1.28	0.55	0.99	0.51	0.72	0.51	2.02	2.42	0.39	0.16
Na_2O	1.20	0.12	3.63	0.07	4.03	0.60	2.43	1.49	2.12	1.35	3.42	0.65	3.98	0.43	3.25	0.60	4.79	0.55	4.18	0.59
K_2O	6.56	0.69	2.62	0.16	4.46	0.86	6.03	1.45	5.25	1.95	6.15	0.92	5.24	0.34	4.67	1.13	3.44	1.15	5.24	0.39
TiO_2	0.89	0.13	1.22	0.00	0.73	0.18	0.48	0.05	0.73	0.16	0.62	0.03	0.51	0.08	0.61	0.06	1.14	1.06	0.51	0.04
MnO	0.06	0.00	0.20	0.00	0.12	0.06	0.09	0.02	0.12	0.03	0.18	0.03	0.15	0.02	0.13	0.01	0.15	0.07	0.12	0.04
P_2O_5	0.22	0.15	0.51	0.01	0.20	0.09	0.07	0.01	0.09	0.03	0.08	0.01	0.08	0.04	0.06	0.02	0.22	0.27	0.05	0.01
ppm																				
Ni	8	0	4	1	3	0	11	4	5	2	5	2	5	1	5	0	5	2	4	1
Cr	8	0	4	0	2	0	12	2	5	4	3	1	3	1	3	0	3	1	4	2
V	36	18	27	0	20	9	19	5	29	23	25	8	14	3	25	6	24	10	12	2
Sc	9	2	5	0	7	2	11	1	7	4	5	1	5	1	6	1	6	1	5	0
Cu	2	1	2	1	0	0	13	15	4	5	4	2	1	1	1	1	2	3	2	3
Zn	155	18	86	1	156	6	188	46	184	23	167	33	179	11	132	11	195	44	161	22
Ga	28	1	14	1	30	1	30	4	30	3	29	2	31	1	24	2	29	9	30	3
Pb	8	1	5	1	14	1	17	2	13	1	13	2	16	2	11	1	13	2	14	2
Sr	194	175	185	5	90	50	147	33	404	255	83	17	37	13	75	71	140	89	50	12
Rb	121	18	69	1	141	37	113	16	127	44	115	11	121	7	89	24	98	29	118	19
Ba	562	11	286	1	844	239	1050	455	826	305	823	175	350	105	532	188	650	273	596	351
Zr	870	101	486	3	881	27	798	56	800	111	809	30	1014	56	834	45	903	203	878	91
Nb	111	14	63	0	100	5	53	4	102	22	108	5	126	7	105	8	116	27	110	22
Th	13	1	7	0	15	1	11	1	13	2	14	1	18	1	14	1	15	4	15	3
Y	71	14	43	1	77	3	81	5	76	8	80	3	87	5	74	6	81	19	82	9
La	83	13	48	3	96	2	77	7	91	17	93	3	93	10	97	11	94	7	105	21
Ce	180	21	101	3	208	8	149	19	200	35	204	16	211	14	200	6	209	18	211	41
Nd	99	13	56	3	98	5	80	11	98	15	102	4	101	8	98	10	102	6	99	14

Analyses were normalized to 100% volatile free, then averaged. Analyses were performed by the first author at Royal Holloway University of London by XRF analysis (please see the Analytical Methods appendix). N = number of sample analyses used in average calculation, sect. = the number of stratigraphic sections samples are derived from. Standard deviation of each element is ±2%, and is listed beside each analysis in the "2 sd" column. This average uses normalized major element totals for all analyses screened for loss on ignition of less than 5 wt.%

Table 3 Summary of key geochemical features and isotope ratios for main units, Oligocene flood volcanism, Yemen

Unit (from youngest to oldest)	Pb group*	$^{207}Pb/^{206}Pb$	$^{208}Pb/^{206}Pb$	$^{143}Nd/^{144}Nd_i$	eNd	Key major and trace element characteristics
Bayt Mawjan Ignimbrite	High	0.826	2.04	0.51286	4.5	Lowest Fe_2O_3
Bimodal volcanics (isotope data from two ignimbrites)	Igs: high tuff + lava: low	0.832 0.825	2.06 2.04	0.51286	4.7	
Haddah Section	High	0.830	2.06	0.51285	4.5	
Iftar Alkalb	High	0.833	2.06	0.51282	3.9	Similar to Sam L zoned to trachyte
Sana'a Ignimbrite	Low	0.813	2.01	0.51288	4.9	Similar to top of Sam U
Sam Upper Ignimbrite	High to low zoned	0.814	2.02	0.51289	4.9	Highest Zr and Nb zoned in many elements and isotopes
Sam Lower Ignimbrite	High	0.832	2.06	0.51282	3.8	Zoned in many elements and isotopes
Green Tuff	High	0.833	2.06	0.51283	3.9	Similar to Sam L
Escarpment Ignimbrite	Crustal melt	0.831	2.04	0.51268	0.9	Highest Fe_2O_3, Pb lowest MgO, TiO_2, Th and Nb
Akraban Andesite	Crustal melt	0.839	2.06	0.51263	0.4	Resembles Esc. Ig, $SiO_2 = 60$ wt%
Jabal Kura'a Ignimbrite	Low	0.812	2.00	0.51286	4.7	Highest Ba
Fine-grained tuffs above SK Ig	–	0.810	2.00	–	–	
Shibam Kawkabam Ignimbrite	Low	0.815	2.02	0.51290	5.7	Highest MgO, TiO_2 lowest Pb

Analyses were performed by the first author at the Danish Lithosphere Centre by a variety of methods, see Ukstins Peate et al. 2003b for full details. "Pb Group" (column 2) refers to differentiation of units on a plot of $^{208}Pb/^{206}Pb$ versus $^{207}Pb/^{206}Pb$ (Fig. 8a) into two groups of low or high after Ukstins Peate et al. (2003b). These divisions into high and low Pb group are based on in-situ Pb isotope analyses by LA-MC-ICP-MS (Ukstins Peate et al. 2003b). The Escarpment Ignimbrite and Akraban Andesite fall off the main Pb isotope ratio trends (Fig. 8a) and represent a distinct component of crustal melting, which will be discussed in detail in a future publication focusing on the petrogenesis of these magmas

tinct (crystal-rich cpx-phyric basalts), and they appear to be stratigraphically unrelated to any lavas found in the Sana'a area. A further 25 km to the west, in the Wadi Lahima section in the coastal rift mountains (Fig. 1: Baker et al. 1996a, b), the basaltic succession attains thicknesses >1,500 m with ~100 flows. It comprises block-faulted sequences of basaltic lava flows and basaltic pyroclastic deposits (e.g. tuffs, bomb beds: Ross et al. 2005), immediately overlying lateritized sandstone basement of the Tawilah Group. Extensive block faulting and rotation precludes construction of a composite volcanic stratigraphy that might directly correlate this section with the Sana'a volcanic stratigraphy. These lavas have normal polarity (Riisager et al. 2001), and combined with stratigraphic evidence are thus inferred to be older than the reversely magnetized lowermost basalts exposed in the Sana'a area. The increase in number and thickness of basaltic lava flows from east to west suggests that the vent sites for initial basaltic volcanism were located towards the Red Sea proto-rift. The mafic volcaniclastic deposits underlying and intercalated with the earliest lava flows potentially record discrete and localized episodes of volcanic activity, such as those observed in the earliest stages of flood volcanism in other large igneous provinces such as East Greenland (Ukstins Peate et al. 2003a), the Paraná-Etendeka (Jerram et al. 1999) and the Ferrar (Elliot 2000).

The oldest dated lava flow in northern Yemen, from near the base of the succession of the Shibam Kawkabam section (Fig. 2), is 30.3 ± 0.2 Ma (Riisager et al. in press), while the observed polarity transition in the paleomagnetic data indicates that initial basaltic volcanism in the Wadi Lahima area is older. In southern Yemen, the earliest flood basalts give a $^{40}Ar/^{39}Ar$ age of 30.9 ± 0.3 Ma (Baker et al. 1996a), and in Ethiopia, volcanism began prior to 31.0 Ma ($^{40}Ar/^{39}Ar$: Ukstins et al. 2002). While the ages of the first dated lava flows across the province are similar, when the underlying basaltic lava succession is taken into account (as in Ethiopia, Ukstins Peate et al. 2003), the initiation of flood volcanism appears to be asynchronous and initiated earlier in Ethiopia and western Yemen (Wadi Lahima) than in northern Yemen. In the Sana'a area, the main phase of flood basalt effusion had a duration of 0.57 ± 0.30 Ma.

Several thin (<2 m) silicic tuffs occur higher in the stratigraphy, above the Shibam Kawkabam Ignimbrite, (Shibam Kawkabam and Jabal Shahirah sections: Fig. 2). These minor tuffs are highly laterally discontinuous, usually forming thin lenses in concave depressions among lobate basaltic lava flows. Most primary volcanological textures have been obliterated due to pervasive alteration to clay, but there is rare evidence for shard morphologies and feldspar crystals in thin section. These units probably represent reworked deposits of distal silicic airfall tuffs, and as such preserve evidence for intermittent silicic eruptions during basaltic flood volcanism.

In the Sana'a area the end of the initial phase of mafic volcanism is marked by the Kura'a Basalt, a distinctive highly plagioclase-phyric lava flow that can be correlated over >30 km. Following this, evidence for a hiatus in volcanic activity or periods of nondeposition or erosion is represented by several epiclastic deposits (~15 m of fluvial sediments, some containing silicified logs up to 1 m long) in the Jabal Shahirah section (Fig. 2). The eruptive products are also more heterogeneous during this waning stage of basaltic volcanism, as seen by the emplacement of two silicic lava flows, a thin (0.3 m) biotite-bearing tuff, and the Akraban Andesite (Jabal Shahirah section: Fig. 2). Baker et al. (1996a) dated a biotite-phyric tuff from the lower part of the volcanic section in southwestern

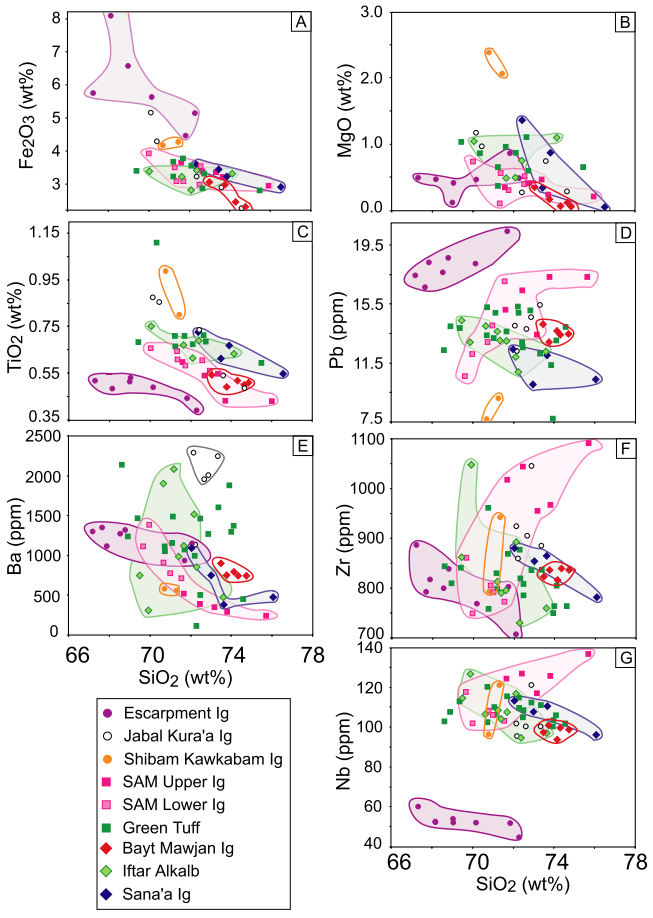

Fig. 5 Harker variation diagrams of SiO_2 versus major and trace element concentrations for the main silicic units. Data fields for all ignimbrites (excluding the Green Tuff) are outlined to show variations within individual eruptive units. Note that Sam U and L have been outlined together but are shown in different colored symbols. Data have been screened for LOI <5%, and data are normalized to 100% totals. See supplemental data for a full dataset and online appendix of stratigraphic sections for full sample descriptions and location information. LOI values are available in the online dataset and specific examples of analyses with high LOI (>5 wt.%) are illustrated for the Green Tuff and Iftar Alkalb in Fig. 3C and D

Yemen that may be equivalent to this tuff unit (J14B: 29.71 ± 0.16 Ma). Elsewhere on the northern Yemen plateau, the transition from mafic flood volcanism to silicic pyroclastic volcanism is marked by the emplacement of silicic tuff and ignimbrite onto mafic lava, with no apparent erosional surfaces between the units (Escarpment and Jabal Kura'a sections: Fig. 2).

Shibam Kawkabam Ignimbrite (30.16 ± 0.13 Ma, 15°25.0′ N, 044°05.6′ E)

This is the oldest ignimbrite found in Yemen, and has been geochemically correlated to the oldest identified ignimbrite within the Ethiopian Traps ($^{40}Ar/^{39}Ar$ age = 30.16 ± 0.13 Ma: Ukstins et al. 2002; Ukstins Peate et al. 2003b). In Yemen this unit is only found in the Shibam Kawkabam section (Fig. 2), where it is preserved as an erosional remnant within a more complete basaltic stratigraphic section. The ignimbrite forms a lens approximately 6 m wide by 3 m thick in a concave depression between two basaltic lava flow lobes. It is unwelded, but indurated and lithified, and is capped by a ~0.4 m thick massive, laterally discontinuous, well-sorted and graded clast-supported unit which is rich in broken feldspar crystals that appear to be derived from the underlying ignimbrite. The upper unit is interpreted as an epiclastic sediment based on its depositional characteristics, laterally restricted depositional area and the obvious erosion of the underlying ignimbrite. The eroded upper portion of the ignimbrite and overlying sedimentary unit suggest that this ignimbrite was originally a more laterally continuous feature. In Ethiopia, the correlated unit is approximately 15 m thick, whereas the total thickness in Yemen is unknown. Both the Yemen and Ethiopian exposures of this unit contain 3 to 5 modal percent of pervasive, highly vesicular, more mafic scoria (from 0.5 to 4 mm, ~58 wt.% SiO_2: Ukstins Peate unpubl. data), which appears to be a primary juvenile clast component of the eruption rather than reworked accidental lithics as evidenced by the preservation of the delicate scoriaceous textures (Fig. 4A) and their ubiquitous occurrence over the entire run-out length of the ignimbrite, as well as in correlated tephra deposits found in Indian Ocean ODP cores (Ukstins Peate et al. 2003b). This unit is geochemically distinguished from other silicic units by its high MgO and TiO_2 (possibly enriched due to the basaltic scoria component), low Pb concentrations, and high εNd values (+5.7: Tables 1–3 and Figs. 5 and 6).

Kura'a Basalt (29.90 ± 0.2 Ma)

This is a highly plagioclase-glomerophyric basaltic lava found in three sections around the Sana'a basin (Fig. 2). It contains abundant feldspar megacrysts (20 to 30%) up to 1.5 cm in size. It ranges from 20 to 30 m in thickness and can be used for stratigraphic correlation among sections covering the upper portions of the main flood basalt eruption phase.

Akraban Andesite (29.61 ± 0.08 Ma)

This is a thick (50–80 m) lava flow that is restricted to the western Sana'a area and immediately overlies the main basaltic lavas (Jabal Shahirah and Bayt Baws sections: Fig. 2). This unit represents a rare example of an intermediate composition rock type in this strongly bimodal province, with SiO_2 of 59.9 wt.% (Fig. 3: Baker et al. 1996b). It has geochemically distinctive features such as low εNd (+0.4) and an anomalously low Nb concentration (32 ppm, see online dataset) separating it from the main group of basaltic lavas and silicic units. Compositionally it is most similar to the Escarpment Ignimbrite, which is stratigraphically one ignimbrite above the Akraban Andesite in the Bayt Baws and Iabal Shahirah sections (Fig. 2, Tables 2 and 3: Baker et al. 1996b; Ukstins Peate 2003).

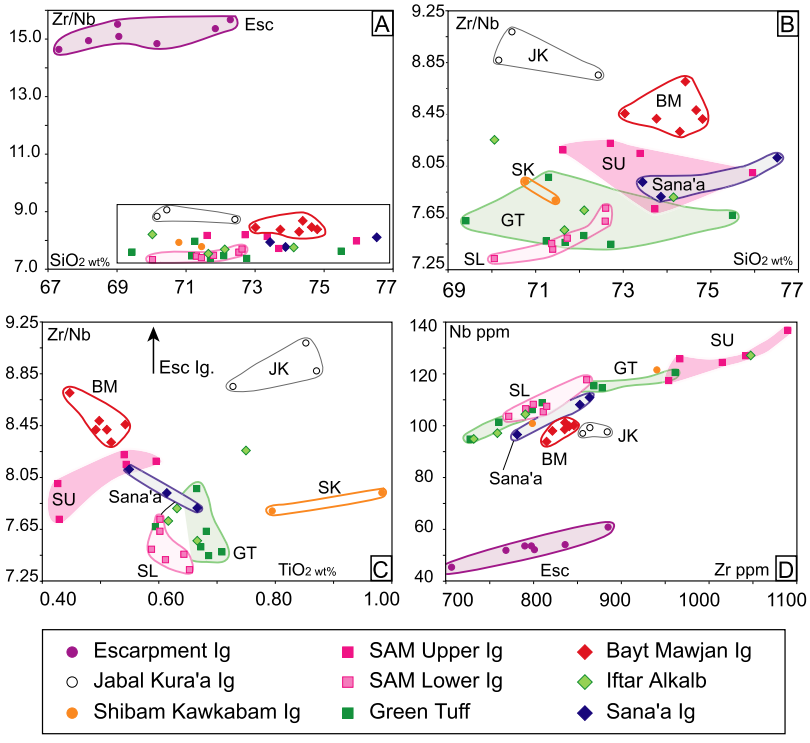

Fig. 6 Major and trace element variation diagrams illustrating geochemical differences among the main silicic pyroclastic units. Data for all units except Iftar Alkalb have been outlined to show variations within individual eruptive units. SiO_2 and immobile trace elements (Zr and Nb) are used here to minimize possible alteration effects. This data set was screened for alteration and samples with LOI >4 wt.% have been excluded. **A**. SiO_2 versus Zr/Nb. The Escarpment Ignimbrite can clearly be differentiated from all the other silicic volcanic eruptive units in Yemen based on the Zr/Nb ratio. **B**. SiO_2 versus Zr/Nb, an enlarged view from Plot A. Jabal Kura'a and Bayt Mawjan Ignimbrites have higher and distinct Zr/Nb ratios than the other ignimbrites shown here. Sam L Ignimbrite has lower Zr/Nb and SiO_2 than Sam U Ignimbrite, which shows little correlation between Zr/Nb and SiO_2. The Green Tuff displays a large spread in Zr/Nb values, but more closely resembles Sam L than Sam U in Zr/Nb ratio. The Sana'a Ignimbrite overlaps Sam U Ignimbrite in terms of Zr/Nb ratio. **C**. TiO_2 versus Zr/Nb. The Shibam Kawkabam Ignimbrite is clearly differentiated from the Green Tuff and Sam Ignimbrites because of its higher TiO_2 at a constant Zr/Nb ratio. Sam U Ignimbrite is also clearly distinct from the Sam L Ignimbrite with higher Zr/Nb and lower TiO_2. **D**. Zr versus Nb. The Escarpment Ignimbrite has elevated Zr/Nb values because it is significantly less enriched in Nb compared to other silicic units. The Green Tuff, Sam L and Sam U all display distinct trends of increasing Zr with increasing Nb (as does the Escarpment Ignimbrite, though at lower Nb); in the Sam Ignimbrites this increase is correlated with stratigraphic height. A similar trend can be observed in the Sana'a Ignimbrite, although the vertical resolution is not well constrained for this unit

Main silicic pyroclastic phase (29.7 to 29.5 Ma)

The second phase of volcanism, the *main silicic pyroclastic phase*, initiated with the emplacement of the Jabal Kura'a Ignimbrite (the first regional ignimbrite found on the northern Yemen plateau) and ended with the emplacement of the Iftar Alkalb mega-breccia. This period of silicic volcanism includes six large-volume pyroclastic flows erupted rapidly over a period of 0.25 ± 0.23 Ma (Fig. 2). The silicic units are rhyolitic, rhyodacitic and trachytic in composition (Fig. 3), and form 20 to 25% of the total Afro-Arabian flood volcanic succession ($>6\times10^4$ km^3: Ayalew et al. 2002; Ukstins Peate 2003). Locally, the silicic units constitute up to 50% of the volcanic stratigraphy of the Yemen plateau. Some of these silicic units have been correlated to ignimbrites found in Ethiopia, and to deep-sea tephra layers found in the Indian Ocean more than 2,700 km away (Jabal Kura'a and Sam Ignimbrites: Ukstins Peate et al. 2003b). The transition from reversely magnetized (main flood basalt phase) to normally magnetized units coincides with the initiation of silicic volcanic activity (Jabal Kura'a and Escarpment sections: Fig. 2; Riisager et al. 2001). The main silicic pyroclastic phase is further identified by a brief transition to reversed polarity recorded by the Sana'a Ignimbrite, and a return to normal paleomagnetic polarity for the Iftar Alkalb mega-breccia (Fig. 2). The erosive nature of the Iftar Alkalb basal contact and this unit's relationship to laterally adjacent basaltic lava flows in the Sana'a area, the Haddah section, and a basaltic mega-breccia found in the Escarpment section (Fig. 2) add stratigraphic complexity to the interpretation of this phase of volcanic activity, as discussed below.

Jabal Kura'a Ignimbrite (~29.6 Ma, 15° 28.8′ N, 044° 25.0′ E)

This ignimbrite, which has not been directly dated, is found in all sections in the Sana'a area (Figs. 2 and 7). Its upper contact varies from conformable to the east to sharply erosional (ca. 1 m relief) to the west. It is welded and varies in color from a pink oxidized groundmass with flattened, green pumice clasts (~2 cm), to a light brown groundmass

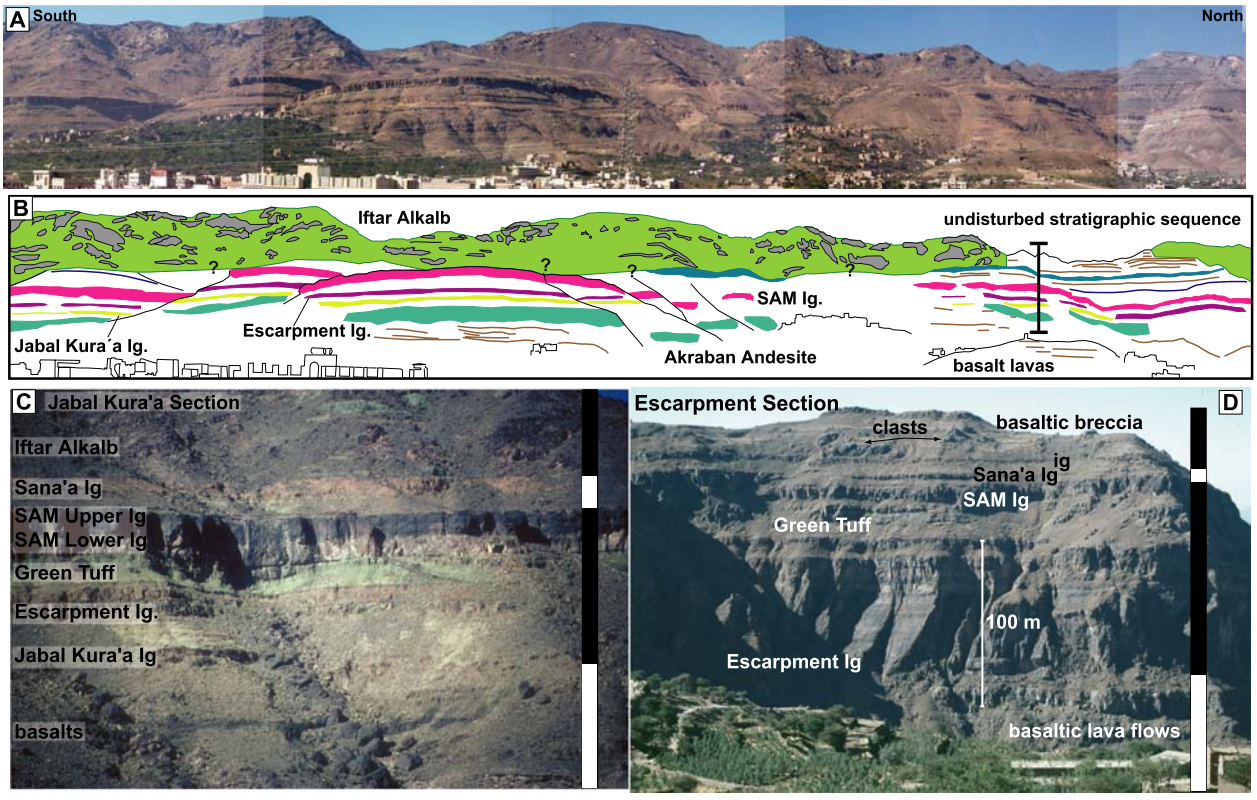

Fig. 7 **A**. Composite photograph of the western side of the Sana'a basin near Haddah, preserving an apparent near-complete volcanic stratigraphic succession from the Akraban Trachyandesite through Sam Ignimbrites and overlying volcanic units (undisturbed stratigraphic section in the northern part of the photographed area). **B**. A schematic stratigraphic interpretation of the composite section shown in Figure 6A. Note the stratigraphically coherent blocks capped by Sam Ignimbrite that are down-dropped into the Sana'a basin (center of photograph). The nonconformable basal contact of Iftar Alkalb is well exposed in the northernmost part of the composite photograph, although it was not accessible in the field due to military restrictions. The undisturbed stratigraphic sequence shown in the northern part of composite photo A represents a volcanic stratigraphic succession that has not been disturbed by the emplacement of the younger Iftar Alkalb megabreccia. **C**. Field photograph of the Jabal Kura'a section showing the volcanic stratigraphy of the lowermost basaltic lavas through the Sana'a Ignimbrite with the overlying Iftar Alkalb. The lower contact of Iftar Alkalb is sharp and planar at this locality. Note the reversed magnetic polarity (*white on black and white bar*) of the Sana'a Ignimbrite, also shown in Fig. 6D. **D**. Field photograph of the Escarpment section showing the volcanic stratigraphy comprising clinopyroxene-phyric basaltic lavas at the base of the section, the thickened Escarpment Ignimbrite (100 m), and overlying silicic units, capped by an unnamed basaltic breccia. Clasts annotated on the photo, part of the mafic volcaniclastic mega-breccia (Fig. 2) represent underlying lithologies such as the Sam Ignimbrite (one block preserved the textural contact between Sam L and Sam U, but was overturned), clinopyroxene-phyric lavas, and clasts of intermediate-composition lavas

with small pumice fragments (<1 cm, Table 1). It is not preserved in the Escarpment section to the west (Figs. 2 and 7), and may have been removed by erosion. It has similar major element compositions to the Shibam Kawkabam Ignimbrite, but has higher Zr/Nb ratios (Fig. 6, Tables 2 and 3), and has the highest Ba content of any Yemen silicic volcanic rocks (Ba = 865 to 2,256 ppm, see online dataset). While this elevated Ba may be a secondary feature, it is consistently found in multiple samples throughout the Sana'a plateau. The Jabal Kura'a Ignimbrite belongs to the "low $^{208}Pb/^{206}Pb$" group (Table 3 and Figs. 5 and 6: Ukstins Peate et al. 2003b).

Escarpment Ignimbrite (~29.6 Ma, 15° 09.6′ N, 043° 56.7′ E)

This unit shows significant lateral thickness variations from >100 m thick in the Escarpment section (Figs. 2 and 7) to 5 to 10 m in the Sana'a area. Several of the overlying silicic pyroclastic units (both ash flow and airfall deposits) also show east to west increases in thickness, albeit to a much lesser extent, despite inferred eruption sources in the Sana'a area (see below), indicates that there may have been significant pre-existing topographic variations before the main phase of silicic volcanism commenced. The order of magnitude east to west thickening observed in the Escarpment Ignimbrite is significantly greater than that exhibited by the overlying silicic units (Fig. 2), and probably also reflects a change from more proximal to distal deposition, with an eruptive source located to the west of the present rift escarpment. Emplacement textures are also laterally variable and may correlate with proximity from vent. In the Escarpment section this unit is densely welded with eutaxitic textures and a thick (3 to 4 m) basal vitrophyre, whereas in the Sana'a area it is unwelded and has no basal vitrophyre. This unit contains ca. 10 to 20% accidental lithic clasts ranging

in size from 0.5 to >10 cm. The largest clasts are generally found in the basal part of the Escarpment section exposure with clast sizes decreasing up-section and laterally eastwards to the Sana'a area, further supporting a postulated vent location to the west of the Escarpment section.

The Escarpment Ignimbrite is compositionally distinct from the other silicic units in terms of major elements. It is classified as a trachyte rather than a rhyolite (Fig. 3), unlike all other unaltered silicic rocks (Tables 1–3, Fig. 6). It is also distinguished by a very high Zr/Nb ratio (14.6 to 15.6 vs. <9), a low Nd isotope ratio ($\varepsilon Nd = +0.9$ vs. +3.3 to +5.7), and an anomalous Pb isotope composition that plots well below the main trend for all other Yemen silicic eruptive units on Fig. 8a ($^{207}Pb/^{206}Pb$ vs. $^{208}Pb/^{206}Pb$).

Green Tuff (29.59 ± 0.12 Ma, 15°16.5′ N, 044° 11.3′ E)

This unit forms a visually distinctive green marker horizon in sections throughout the Yemen plateau, and it is always paired with the overlying Sam Ignimbrite (Figs. 2 and 7). It overlies a fluvial conglomerate in the Sana'a area, indicating a period of subsidence and erosion immediately following the emplacement of the Escarpment Ignimbrite. In the Sana'a area it has a thickness of approximately 10 m, thickening by ca. 50% to 20 m in the Escarpment section.

The Green Tuff is composed of devitrified ash shards (0.1 to 0.2 mm) forming a massive, fine-grained, unwelded deposit (Fig. 4B). The primary component of ash shards is highly restricted in the range of small shard diameters present, but does not appear to show any sorting within the deposit. This could be due to the difficulty in recognizing grain size changes within such a small range of shard sizes. Euhedral and broken feldspar (anorthoclase, up to ~0.7 cm, some with sieve texture) are common throughout, and display normal sorting up-section within the unit. Small augite phenocrysts are present (1 to 2%). Very rare charred wood fragments (from ~0.5 cm to >1 m; Kruck et al. 1996), pumice and accidental lithic clasts of basaltic lava and ignimbrite are also present, particularly in the basal parts. The upper contact with the Sam Ignimbrite is always sharp and planar, with no evidence for any time break in the form of erosional surfaces, epiclastic sediments or paleosols developed between the two units. Because of the extremely fine-grained nature of the ash shards and the subtle normal grading of feldspar phenocrysts within the unit, coupled with the relatively constant thickness over the Sana'a area and lack of any bedding textures or layers within the unit, we interpret the Green Tuff as representing a pyroclastic airfall deposit produced from a magmatic eruption. Based on stratigraphic and geochemical relationships, the Green Tuff is inferred to be the preliminary airfall deposit preceding eruption column collapse (Freundt et al. 2000) and emplacement of the overlying Sam Ignimbrite (see below).

More than half of the 20 analysed samples from this unit have high loss on ignition values (6 to 13 wt.%, Fig. 3C) due to hydration and alteration of the ash matrix, as well as apparent alkali loss due to alteration (Fig. 3). Samples with loss on ignition <5.2 wt.% show a range in SiO_2 (68.9 to 74.5 wt.%: Fig. 5) with a trend of increasing SiO_2 content with increasing stratigraphic height, indicating that this unit is reversely zoned. The range observed in major and trace element concentrations, and the homogeneous values for Pb and Nd isotope ratios, overlaps the composition of the overlying Sam Lower Ignimbrite (Figs. 5, 6 and 8).

Sam Ignimbrite (29.47 ± 0.14 Ma, 15° 6.5′ N, 044°11.3′ E)

The Sam Ignimbrite forms a prominent capping horizon throughout the volcanic plateau in the Sana'a area. It has been geochemically correlated to exposures in Ethiopia, and to tephra layers in ODP Leg 115 drill cores from the Indian Ocean (Ukstins Peate et al. 2003b), making this the Afro-Arabian silicic unit with the largest currently recognized areal distribution. The $^{40}Ar/^{39}Ar$ age used here represents an isochron age from two sanidine single-crystal step heating experiments (Ukstins et al. 2002). This may be the same unit referred to by Heyckendorf and Jung (1991) as the "*...Plateau Ignimbrite: a prominent marker horizon comprising two units...*" but their generalized stratigraphy and limited field descriptions preclude definite correlation.

The Sam Ignimbrite is a strongly welded, dark pink unit that is easily recognized in the field by a prominent vertical textural change in outcrop appearance (Figs. 4C and 7C). The ignimbrite is divisible into a lower unit (Sam Lower or L) that is massive and fine-grained (<0.05 mm) although exhibiting a slight coarsening upward trend from a very fine-grained base (0.01 mm), and an upper unit (Sam Upper or U) that has an ~0.5 m thick very fine-grained base (0.01 mm) resting directly on Sam L, above which is a prominent vertical platy jointing (~10 cm spacing) throughout the unit. All outcrops of the Sam Ignimbrite show these two textural units, and there is no evidence for any erosion between them. This unit contains anorthoclase, augite and ilmenite phenocrysts (ca. 2–4% total), with augite phenocrysts becoming more abundant up-section within the unit. The Sam Ignimbrite is approximately 16 m thick in the Sana'a area and increases to about 25 m in the Escarpment section (Fig. 2). The top of Sam U is eroded in the Jabal Kura'a and Jabal Shahirah sections. In areas where the entire unit is preserved (Bayt Baws and Escarpment section), however, Sam L and Sam U are subequal in thickness. Welding and compaction are the same throughout the ignimbrite, with no obvious changes between Sam L and Sam U (Figs. 4C and 7). The Sam Ignimbrite may represent two eruption units that were emplaced in rapid succession and cooled as a single massive unit (i.e. compound cooling unit of Smith 1960).

A diagnostic geochemical characteristic of the Sam Ignimbrite is the zonation observed in both elemental concentrations and radiogenic isotope ratios (Tables 1–3, Figs. 5, 6 and 8). SiO_2, Zr, Nb and Th contents increase progressively with increasing stratigraphic height, while TiO_2, MgO, and Ba contents decrease (Fig. 8D and E). Pb isotope ratios change abruptly within the ignimbrite, where Sam L and

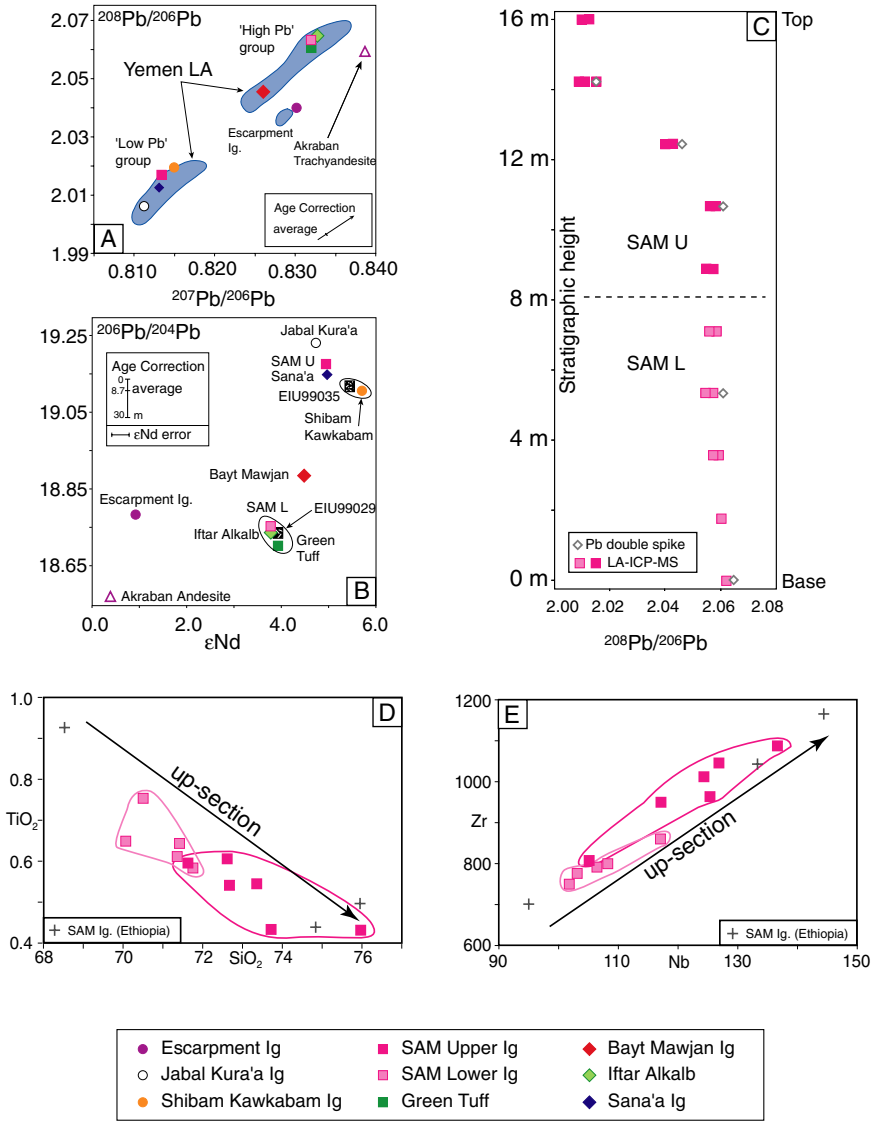

Fig. 8 Isotope ratio variation diagrams showing isotopic differences amongst the main silicic units. **A**. $^{207}Pb/^{206}Pb$ versus $^{208}Pb/^{206}Pb$ isotope variation diagram showing the full Yemen dataset of in situ Pb isotope LA-MC-ICP-MS analyses (*blue fields* on Fig. 8A, marked "Yemen LA") representing a significant dataset of silicic units (data available in online dataset associated with Ukstins Peate et al. 2003b). Pb isotope analyses of individual units by double spike methods have also been plotted (one analysis per unit, Ukstins Peate et al. 2003b). The Green Tuff, Sam L Ignimbrite, Iftar Alkalb and Bayt Mawjan Ignimbrite lie in the 'high Pb' field, whereas the Shibam Kawkabam, Jabal Kura'a, Sam U and Sana'a Ignimbrites lie in the 'low Pb' field. The Escarpment Ignimbrite lies off the main Yemen trend. **B**. $^{206}Pb/^{204}Pb$ versus εNd isotope variation diagram showing isotopic correlations among the main Yemen silicic units and two Ethiopian ignimbrites (EIU99029 and EIU99035, described in Ukstins Peate et al. 2003b). **C**. In situ Pb LA-MC-ICP-MS and Pb double spike analyses on groundmass chips from a detailed drilling profile (16 m) through Sam Lower and Upper Ignimbrite showing the absolute variation in Pb isotope ratio with stratigraphic height. **D**. SiO_2 vs. TiO_2 variation diagram showing concentration variations within the Sam Lower and Upper Ignimbrite from Yemen (*filled squares*) and Ethiopia (*plus signs*). There is a negative correlation with TiO_2 decreasing as SiO_2 increases with increasing stratigraphic height within the ignimbrite. **E**. Nb vs. Zr variation diagram showing concentration variations within the Sam Lower and Upper Ignimbrite from Yemen (*filled squares*) and Ethiopia (*plus signs*, Ukstins Peate 2003, data included in supplemental dataset). Ethiopian samples are from the lower, middle and upper part of the unit, which is 15 m thick at the Kuta Ber locality, Ethiopia (Ukstins et al. 2002). A positive correlation exists between increasing Nb and increasing Zr concentrations with increasing stratigraphic height within the ignimbrite throughout its areal extent

the lowest 2/3 of Sam U plot in the "high $^{208}Pb/^{206}Pb$" group, while the top 2 to 3 m of Sam U plots in the "low $^{208}Pb/^{206}Pb$" group (Ukstins Peate et al. 2003b). This distinct and sharp geochemical transition does not correspond with any textural breaks in the unit (Fig. 8C). Nd isotope ratios change in tandem with Pb isotope ratios.

Ukstins Peate et al. (2003b) correlated the Sam Ignimbrite to a unit in the Kuta Ber section of Ethiopia (Fig. 1) that shows identical elemental and isotopic zonation. The textural changes seen in the Yemen exposures, however, are not present in the Ethiopian outcrop where the entire 15 m thickness of the unit is unwelded. The compositional

zonations observable over the full lateral extent of the ignimbrite (Yemen and Ethiopia) provide support for a depositional mechanism of progressive aggradation (Branney and Kokelaar 2002). In addition, the continuous compositional zonation up-section within the Sam Ignimbrite, which crosses the textural boundary used to differentiate Sam L and Sam U, and the lack of any erosional contact or break within the ignimbrite, indicates that the observed grain-size variations may reflect variable conditions within a single eruption column rather than emplacement of multiple eruptions (Branney and Kokelaar 2002).

Sana'a Ignimbrite (~29.5 Ma, 15° 28.8′ N, 044° 25.0′ E)

The upper surface of the Sam Ignimbrite is an erosional boundary and in the Jabal Kura'a section it is capped by a laterally discontinuous fluvial conglomerate containing well-rounded volcanic cobbles up to ~30 cm in diameter. The Sana'a Ignimbrite (Fig. 4C) overlies this fluvial conglomerate, but no conglomerate clasts were incorporated into the ignimbrite. This suggests that either the epiclastic deposit was relatively well consolidated prior to eruption, or that the ignimbrite flow energy was not significant enough to incorporate the cobbles. In the Escarpment section, the erosional upper surface of the Sam ignimbrite is directly overlain by the Sana'a Ignimbrite (Fig. 2). Elsewhere in the Sana'a area the Sana'a Ignimbrite is not preserved in the stratigraphic succession (Bayt Baws and Jabal Shahirah sections: Fig. 2), and presumably was removed by erosion possibly associated with the emplacement of the overlying Iftar Alkalb mega-breccia.

Where preserved, the Sana'a Ignimbrite is approximately 5 m thick, and thinner than all other main silicic ignimbrite units. It has a characteristic orange-weathering color and it is uniquely identified by its reversed magnetic polarity (Figs. 2 and 7: Riisager et al. 2001). In thin section, this unit contains abundant, brown glassy blebs (0.1 to 2.0 mm) that may represent a more mafic component such as that observed in the underlying Sam Ignimbrite and correlated tephra layers (Fig. 4D). The Sana'a Ignimbrite unit has the highest average SiO_2 content of the main silicic units (SiO_2 = 74.6 wt.%, Fig. 3), with Pb and Nd isotope ratios that are identical to the isotopically distinctive top of the Sam U Ignimbrite (Fig. 8). Based on the isotopic similarities between the top of Sam U and the Sana'a Ignimbrites, we postulate that these eruptions were geochemically related, originating from the same eruptive center possibly as part of the same eruptive sequence. Stratigraphic evidence indicates that there was a hiatus in volcanism between emplacement of the Sam and Sana'a Ignimbrites although $^{40}Ar/^{39}Ar$ age data for the Sam Ignimbrite and overlying Iftar Alkalb megabreccia (29.47 ± 0.14 and 29.48 ± 0.13, respectively: Table 3) bracket the Sana'a Ignimbrite and indicate that all these eruptions took place in rapid succession (ca. 0 to 280 kyr).

Laterally adjacent to Iftar Alkalb in the Sana'a area is a sequence of volcanic units observable in Fig. 7A. Due to military restrictions, these sections are not accessible. Baker (1996) had access to equivalent sections in the Sana'a area and reported that Iftar Alkalb laterally abuts a 100 m thick series of coherent mafic lava flows (basalt, hawaiite and basanite). These units must have been erupted prior to emplacement of Iftar Alkalb, and are therefore considered part of the main silicic phase. Little is known about their stratigraphic relationship to other, accessible sections that do not preserve any basaltic lavas during this phase of volcanism.

Iftar Alkalb mega-breccia (29.48 ± 0.13 Ma, 15° 16.5′ N, 044° 11.3′ E)

This unit is interpreted as a caldera collapse breccia, probably derived from an unrecognized caldera in the Sana'a area (Figs. 2 and 7). It is an ash-matrix-supported breccia that extends outward from the Sana'a area up to ~30 km (to Jabal Kura'a section, Fig. 2) and ranges from 70 to >150 m in thickness. Accidental lithic clasts of underlying lithologies (such as Sam Ignimbrite and Kura'a Basalt) comprise 5 to 15% of the deposit, ranging from sand-sized material to massive blocks 30×70×20 m (Fig. 7). Basaltic clasts range from blocky massive lavas (up to 10's of m) to fluidal, ribbon-like stringers up to 3 m long, and are interpreted to represent both accidental and juvenile clasts, respectively. Some blocks (mafic and silicic) have striated surfaces (Fig. 4E) that are interpreted as slickensides formed when blocks collide in a moving pyroclastic flow (e.g. Calder et al. 2000). The juvenile matrix is composed of ash shards and vesicular pumice (up to 3 cm, Fig. 4F), with euhedral megacrysts of feldspar (up to 1 cm), "jigsaw phenoclasts" (Fig. 4G, Best and Christiansen 1997), and cored bombs (up to 20 cm). Accretionary and armored lapilli were only recognized in the Jabal Kura'a section (Fig. 4H), and occur in a laterally restricted sequence (about 3 m thick) in the lower half of the unit.

The lower contact of the breccia unit is a nonplanar surface that cuts down-section into the stratigraphy (Fig. 7A), although not below the top of the Sam Ignimbrite. Exposures of the flood volcanic succession immediately to the west of the Sana'a basin show this nonconformable lower contact (Fig. 7A and B). These exposures also show listric-faulted slump blocks representing stratigraphically coherent sections from the lowermost Akraban Andesite lava through to the Sam Ignimbrite that form a scallop-shaped fault-bounded edge around the western Sana'a basin (Fig. 7A). Due to the highly variable nature of this contact both laterally and vertically, and the lack of any erosional sedimentary features along the contact (i.e. conglomerates or other sediments), we interpret this basal contact as a primary feature of the unit that occurred during emplacement, and not due to pre-existing erosion of the stratigraphy. The primary pyroclastic textures, the clasts and megaclasts of underlying lithologies, unit thickness and laterally restricted deposition are characteristic features of caldera collapse breccias (Lipman 1976; Hargrove and Sheridan 1984; Thompson 1985; Branney and Kokelaar 1994; Dadd

1998). Based on the fault blocks observable on the western edge (Fig. 7) and on the distribution of Iftar Alkalb around the Sana'a basin itself the Sana'a basin may represent the source caldera for Iftar Alkalb. Further work mapping out the detailed distribution of Iftar Alkalb and the contact relationships of the lower surface with the surrounding stratigraphy could test this hypothesis and refine the location for the source caldera.

The Iftar Alkalb ash matrix has a significant range in SiO_2 with the majority of analyses about 68 wt.% (LOI $< 5\%$, $n = 5$). Two samples of matrix from the lower and upper part of the Jabal Kura'a section (Fig. 2) yielded SiO_2 of 61.9 and 51.9 wt.%, respectively (Fig. 3, LOI = 4.4 and 5.6, see supplemental data). This evidence for complex zoning in major elements was not observed in the Bayt Baws section. Only the more silicic samples are plotted for comparison with other silicic tuffs on Figs. 5 and 6.

In situ Pb isotope ratios are identical for all groundmass samples of Iftar Alkalb, and Pb and Nd isotope ratios are the same as the underlying Green Tuff and Sam L Ignimbrite (Table 3). Major and trace element compositions for the Iftar Alkalb matrix span the approximate range seen in the Green Tuff and Sam L Ignimbrite (Figs. 5, 6 and 8). A more detailed discussion of the geochemical zonations of Iftar Alkalb, as well as other units described here, will be presented in a future publication on the petrogenesis of Afro-Arabian silicic volcanism. The compositional zonations observed in major and trace elements, however, complicate efforts to correlate Iftar Alkalb to any related caldera outflow deposits based solely on geochemical parameters. There are several minor ignimbrites in the Haddah and Escarpment sections that may be related to Iftar Alkalb (Fig. 2), but without further detailed field mapping to constrain lateral relationships among units we are unable to establish stratigraphic correlations at this time.

It is unclear how the mafic breccia in the Escarpment section relates to the volcanic stratigraphy in the Sana'a area, and whether it is a primary volcanic feature related to the emplacement of Iftar Alkalb in the east. Further detailed field work is necessary to constrain the lateral stratigraphic relationships of this unit beyond its brief description herein. This unit, like the Iftar Alkalb, contains clast and megaclasts of underlying lithologies such as Sam Ignimbrite, intermediate lavas, and clinopyroxene-phyric basaltic lavas. Sources for the breccia clasts are different from those found in Iftar Alkalb reflecting the distinct clinopyroxene-phyric mafic lavas found in the basal Escarpment succession. Clasts range in size from several cm up to 5 m and are supported in a mafic ash matrix containing euhedral and complexly zoned clinopyroxene crystals (Fig. 4I). This unit is massive and matrix supported. Based on the lack of observed sedimentary features such as fluvial channels, grading or sorting of the deposit, and the presence of mafic ash with euhedral clinopyroxene crystals, we interpret it as a volcanic deposit.

Upper bimodal phase (29.5 to ~27.7 Ma)

The final phase of flood volcanic activity, the *upper bimodal phase*, is defined as the succession of units that are younger than the Iftar Alkalb mega-breccia (29.48 Ma). It is a laterally heterogeneous and lithologically highly variable sequence of thin silicic lavas, tuffs and ignimbrites (generally <10 m), intermediate and basaltic lavas and volcaniclastic units, with sedimentary sequences and erosional surfaces present. The thickness of this sequence varies from 30 to >60 m, and it is capped by the thick (30 to 60 m), eutaxitic Bayt Mawjan Ignimbrite (27.67 ± 0.12 Ma) that is exposed throughout the northern Yemen plateau at the highest stratigraphic level. The upper bimodal phase immediately underlying the Bayt Mawjan Ignimbrite in the Jabal Kura'a and Bayt Mawjan sections preserves a second phase of reversed magnetic polarity, recorded in a sequence of tuffs, ignimbrites and a silicic lava (Fig. 2). These reversely magnetized units are missing from the westernmost Escarpment section, either because they were never emplaced there or, more likely, because they were removed by erosion.

Most of the silicic units in the upper bimodal phase have phenocryst assemblages of anorthoclase, ilmenite, magnetite, ± quartz, and, for the first time in the eruptive sequence, hydrous phases of amphibole (magnesiokatophorite and richterite: Ukstins Peate unpubl. data) are observed in the silicic units (Fig. 4J). One exception is a thin (<1 m) biotite-phyric tuff found in the Jabal Shahirah section immediately underlying the Akraban Andesite (Fig. 2). The common occurrence of primary hydrous phases in the upper part of the stratigraphy suggests increasing degrees of fractionation and volatile saturation of silicic magmas with time. Some of the silicic units contain quartz phenocrysts that show evidence for resorption, and one tuff unit (YIU99121) has resorbed quartz phenocrysts with highly silicic melt filling the embayments (Fig. 4K). This resembles textures described in the Fish Canyon Tuff (USA) which are thought to represent rejuvenation of an upper crustal batholith by injection of a new mafic magma, resulting in remelting and eruption of a partly-solidified magma body (Bachmann et al. 2002).

This final sequence of units is stratigraphically complex and not well constrained because many units occur in only one section. The sequence represents the waning phase of flood volcanic activity and is characterized by small eruptions of hydrous magma from localized volcanic depocenters, as evidenced by the highly variable stratigraphy and compositions. Of the six minor silicic units in the Bayt Mawjam section, three (all ignimbrites) belong to the 'high $^{208}Pb/^{206}Pb$' group and three (two airfall tuffs and a lava flow) belong to the 'low $^{208}Pb/^{206}Pb$' group. This suggests that these units represent intercalated eruptions from multiple eruptive sites. Younger volcanic units have only been located in the north-east Sana'a region. Baker et al. (1996a) investigated a sequence of ~30 mafic lavas that overlie the Bayt Mawjan Ignimbrite at Jabal Ragbaan, ~5 km east of the Jabal Kura'a section. This sequence contains a significant nonconformity juxtaposing two lavas $^{40}Ar/^{39}Ar$ dated at 26.8 ± 0.4 and 19.9 ± 0.6 Ma, which is interpreted as

an unconformity related to the break-up of Africa and Arabia during continental rifting and formation of the Red Sea ocean basin (Baker et al. 1996a).

Bayt Mawjan Ignimbrite (27.67 ± 0.12 Ma, 15° 12.1′ N, 043° 58.8′ E)

This is the youngest of the principle silicic units, and forms a 35 to 50 meter-thick capping ignimbrite throughout northern Yemen (Fig. 2). It is the only ignimbrite that consistently displays a basal vitrophyre (2–3 m thick). The basal vitrophyre shows perlitic cracking and is glassy with densely welded shards and collapsed juvenile spatter clasts (Fig. 4L). It has ~5% phenocrysts including anorthoclase, sanidine, quartz, augite, salite, ilmenite and magnetite. The rest of the unit is dark red, highly welded, and has elongate fiammé up to 20 cm in length. Compared to other units (Figs. 5 and 6), the Bayt Mawjan Ignimbrite has high SiO_2 (~74 wt.%) and the lowest Fe_2O_3 (~2.8 wt.%), and it has higher Zr/Nb ratios and lower Nb concentrations (similar to the Jabal Kura'a Ignimbrite, but not as extreme as the Escarpment Ignimbrite). This unit is subtly distinct from the other units of the 'high $^{208}Pb/^{206}Pb$′ group in having relatively low $^{208}Pb/^{206}Pb$ (Fig. 8A).

Discussion

Eruption volumes and mechanisms

Table 4 presents thickness data and estimated eruption volumes for eight prominent silicic units. Three of these major ignimbrite units (Shibam Kawkabam, Jabal Kura'a and Sam Ignimbrites) have been geochemically correlated to on-land ignimbrites in Ethiopia and/or to deep-sea tephra layers found in the Indian Ocean >2,700 km from the inferred eruption sources in Afro-Arabia (Ukstins Peate et al. 2003b). This extensive area of emplacement has significant implications for estimates of distal ash volumes (e.g. Pyle 1999). Eruption volume estimates are divided into three zones: northern Yemen (Sana'a area plus Escarpment section), Afro-Arabia (northern Yemen plus Ethiopia), and distal deposits that include tuffs found in Indian Ocean drill cores (Table 4). Touchard et al. (2003a, b) have identified the same Indian Ocean tephra layers on a near-global basis (South Atlantic, Italy, Arabian Sea). Volume calculations for the major silicic units are described below. It is important to note, however, that a small but significant percentage of the silicic units found in Yemen are laterally restricted (e.g. upper bimodal ignimbrites and tuff units in Bayt Mawjan section). Without more detailed mapping to constrain the areal distribution of such units it is impossible to provide an accurate estimate of the silicic pyroclastic contribution to the volume of the province as a whole.

Yemen volume estimates were restricted to the northern part only because detailed stratigraphic studies have not yet been carried out in southern Yemen. If future studies conclusively identify silicic units distributed over the entire Yemen flood volcanic field, such as the biotite-bearing tuff found in the main basalt sequence (Fig. 1), minimum eruption volumes for individual units as identified herein would triple in size. Volume estimates presented for northern Yemen are minimum values, taking into account the observed lateral distribution and measured thickness in the studied field area. The Shibam Kawkabam and Jabal Kura'a Ignimbrites are both missing from the Escarpment section but are correlated to units in Ethiopia and the Indian Ocean, implying that these units were once laterally continuous in northern Yemen. For these units, an assumed thickness was used for the Escarpment section based on the observed ca. 50% increase in thickness of other units from east to west (see Table 4 for details of volume calculations). Minimum volume estimates for individual ignimbrites present in northern Yemen range from 70 to 430 km^3 (Table 4). Iftar Alkalb, despite having a restricted depositional area, has an estimated volume of up to ~600 km^3. When the Sam Ignimbrite correlation to Ethiopia is considered, the minimum estimated volume of this ignimbrite over its observed areal extent in Yemen and Ethiopia is ~950 km^3.

Distal ash volumes are difficult to estimate with precision, but a reasonable assumption is that ash layer thickness shows exponential decay (Pyle 1989, 1995, 1999). This method may underestimate the actual volume if the tephra fall deposit contains a significant amount of sub-millimeter sized ash (Bonadonna et al. 1998). Distal ash volumes were calculated using the formula of Pyle (1999: V=3.7AT), assuming a circular isopach at ~3,000 km (which yields an area of 10^7 km^2) and tuff thicknesses based on ODP drill core data (for Jabal Kura'a – 0.10 m, and for the Sam Ignimbrite -0.15 m; Ukstins Peate et al. 2003b). This yields minimum volumes of 3,700 and 5,550 km^3 for distal tuffs associated with the Jabal Kura'a and Sam Ignimbrites, respectively (Table 4). These estimates have a factor of 2 to 3 uncertainty based on assuming a circular isopach, as it was probable that the actual isopach was elliptical and elongated in the direction of the prevailing paleowind. Converting the bulk tephra and on-land ignimbrite volumes to dense rock equivalent (DRE, using a density of 2,000 kg/m^3 for ignimbrite, 1,000 kg/m^3 for ash and 2,400 kg/m^3 for magma) for the Sam Ignimbrite produces an ignimbrite DRE volume of 710 km^3 and a distal ash volume of ~2,400 km^3 for a minimum estimated total volume of 3,100 km^3 (DRE). This is equivalent to a total erupted mass of 7.4×10^{15} kg, a significant size on the scale of the Toba eruption (Rose and Chesner 1987). Estimated minimum total volumes for other prominent silicic units in Yemen range from 52 to 1,630 km^3 (DRE, Table 4).

Depositional features of distal ash layers can also provide constraints on eruption mechanisms. Sustained co-ignimbrite plumes can be responsible for the distribution of ash to distances >1,000 km compared to Plinian eruption columns that tend to distribute tephra to a maximum of hundreds of km from the vent (Sparks and Walker 1977; Moore 1991; Self 1992; Woods and Self 1992; Koyaguchi and Tokuno 1993). Co-ignimbrite ash clouds are entrained from hot, dense pyroclastic flows resulting from collapsed

Table 4 Summary of estimated eruption volumes for main silicic pyroclastic units, Oligocene flood volcanism, Yemen

Unit (youngest to oldest)	Thickness (m)				N. Yemen[a] (km^3)	Afro-Arabia (km^3)	Distal tuffs (km^3)	Total volume DRE (km^3)*	Total mass 10^{12} kg
	Sana'a	Esc	Eth	IO					
Bayt Mawjan Ignimbrite	35	50	–	–	410	–	–	**342**	820
Iftar Alkalb[b]	70 to 150	–	–	–	270 to 580	–	–	**225 to 483**	870
Sana'a Ignimbrite	5	8	–	–	62	–	–	**52**	124
Sam Ignimbrite	16	25	15	0.15	196	946	5550	**3101**	7442
Green Tuff	10	20	–	–	140	–	–	**58**	140
Escarpment Ignimbrite	5	100	–	–	430	–	–	**358**	860
Jabal Kura'a Ignimbrite	7	– (est 15)	–	~0.10	102	–	3700	**1627**	3904
Shibam Kawkabam Ignimbrite	? (est 5)	– (est 10)	10	–	70	570	–	**475**	1140

[a]Northern Yemen volume estimates for units with thickness variations were calculated as 60% by volume at the Sana'a thickness (representing the northern Yemen plateau) plus 40% by volume at the Escarpment section thickness. Thickness data for Ethiopia (Kuta Ber section) and the Indian Ocean (IO) are from Ukstins et al. (2002) and Ukstins Peate et al. (2003b), respectively.

[b]Iftar Alkalb has a restricted areal distribution in the Sana'a area and the volume was calculated based on observed geographic distribution as a circular area using a radius of 35 km. All other units were calculated using a radius of 55 km. These estimates represent minimum areal extent and are based on observed lateral distribution for studied units and the lack of detailed region-wide mapping precludes using true known areal distributions.

Including units that can be geochemically correlated to exposures in Ethiopia and tephra layers found in Ocean Drilling Program cores from the Indian Ocean, Leg 115. Areal extent used in volume calculations for Northern Yemen was 1×10^4 km^2, for Northern Yemen + Ethiopia (correlation to Kuta Ber section, Ethiopia) was 5×10^4 km^2, and correlation to tuffs in the Indian Ocean was 1.4×10^6 km^2, and to distal tuffs in the Arabian and S. Atlantic Oceans (based on magnetostratigraphic studies of Touchard et al. 2003a, 2003b) was 1×10^7 km^2. Calculations for total volume (dense rock equivalent: DRE) use a density of 2,000 kg/m^3 for ignimbrite, 1,000 kg/m^3 for ash and 2,400 kg/m^3 for magma. All volume estimates represent minimum volumes, see text for full discussion

eruption columns, and may originate either close to or at some distance from the vent site. They tend to be enriched in fine vitric ash and rise by convection to as much as 30 km (Woods and Wohletz 1991). Tephra dispersal may also have been aided by stratospheric injection of ash and rapid hemispheric dispersal by winds. Estimates of the amount of pyroclastic material entrained in the co-ignimbrite plume range from 35% up to potentially 100% of the total ignimbrite deposit mass (Woods and Wohletz 1991). Thus, these additional distal facies can contribute a significant extra component to the calculated volumes (Bonadonna et al. 1998). One means of differentiating the relative contributions of co-ignimbrite fall deposits from co-plinian deposits in distal ash units is to quantify the thickness half-distance (b_t of Bonadonna et al. 1998), however these data are not yet available for any Yemen silicic units. The apparent general fine-grained nature of these ignimbrites may also result from highly explosive eruptions (Gardner et al. 1996).

Tectono-volcanic evolution of Afro-Arabian continental rifting

The transition from the main phase of silicic volcanism to upper bimodal volcanism represents a change to smaller, more laterally restricted eruption units consisting of thin tuffs, ignimbrites, and rhyolitic lavas (Bayt Mawjan section, Fig. 2). The estimated eruption interval of units in the main silicic phase ranges from 0 to as much as 300 Ka, and the upper bimodal phase (represented by well-constrained stratigraphy and age data of the Bayt Mawjan section) ranges from about 60 to 120 Ka (Fig. 2). These two eruption phases present a broadly similar range in eruption frequency accompanied by a dramatic decline in eruption volume, estimated to decrease by a factor of 50 following the main phase of silicic volcanism.

This change from large-volume deposits to smaller volume units resembles the difference between the end-member large silicic volcanic systems proposed by Houghton et al. (1995), as represented by Yellowstone (USA) and Taupo (New Zealand). While the averaged magma discharge rates, total thermal fluxes and life spans of the Yellowstone and Taupo volcanic systems are comparable, the styles and sizes of eruptions are different. In general, Yellowstone has long-term magmatic cycles that has produced few, voluminous ignimbrite eruptions, whereas Taupo has an order of magnitude more eruptions, but with significantly smaller eruptive volumes (Houghton et al. 1995). The difference is attributed to the differences in crustal and tectonic characteristics: Yellowstone is located in a stable continental setting where large magma-chambers can evolve over extended periods of time, whereas the Taupo volcanic zone occurs on thin, rapidly extending crust that may result in disrupted magmatic cycles and more frequent eruptions (Houghton et al. 1995). This tectonic disruption may promote effusion of small-volume rhyolites (Axen et al. 1993). The transition observed in Afro-Arabia from early, large-volume silicic pyroclastic deposits that were emplaced on a near-global scale, to smaller, localized eruptions may reflect the initiation of continental rifting and concomitant crustal thinning during break-up. The Whitsunday province, Australia, shows a similar transition from an initial explosive silicic volcanic phase to mixed effusive-explosive eruptions (Bryan et al. 2000).

One means of testing such a model of tectono-volcanic evolution might come from linking individual silicic pyroclastic units to specific intrusive granitic complexes exhumed along the Red Sea escarpment. Geoffroy et al. (1998) have suggested that some of the Yemen Oligo-Miocene granites were emplaced contemporaneously with extension, and were intruded passively into the necked areas of stretched continental crust. It has been proposed that the exhumed granites may represent sources for silicic volcanism (Mohr 1991; Tommasini et al. 1994). Preliminary studies indicate that some granite complexes are isotopically similar to individual silicic units found in northern Yemen (Bayt Mawjan Ignimbrite, Ukstins Peate 2003). If these granites can be compositionally linked to a specific interval of silicic magmatism in the lava stratigraphy, this will further constrain the timing of volcano-tectonic evolution and initiation of continental break-up.

Comparison with the Paraná-Etendeka province

The Early Cretaceous Paraná-Etendeka province is one of the few flood basalt provinces where silicic volcanics have been studied in detail in terms of physical volcanology, composition and eruption size (e.g. Milner et al. 1992, 1995; Garland et al. 1995; Marsh et al. 2001). Most of the silicic units are interpreted to be emplaced as rheoignimbrites that range in thickness from ~20 to >200 m. Several major units have been compositionally correlated across the Atlantic Ocean, and on-land eruptive volumes of individual units can exceed 6,000 km^3 (Milner et al. 1995), in contrast to ~800 km^3 estimated for on-land ignimbrites correlated from Yemen to Ethiopia (this study, Ukstins Peate 2003b).

Both Yemen and Paraná-Etendeka silicic units range from trachytic and dacitic to rhyolitic in composition, but eruption temperatures differ significantly between the two provinces. The Paraná-Etendeka rheoignimbrites were erupted at temperatures >1,000–1,050°C, and are inferred to be relatively low-explosivity events to maintain high temperatures on deposition and facilitate welding, agglutination and rheomorphism (Garland et al. 1995; Ewart et al. 1998). Eruption temperatures for Yemen ignimbrites and tuffs fall between 850 and 1,000°C (Ukstins Peate 2003), and the unequivocal pyroclastic textures, coupled with the large areal distribution of ash fall deposits indicate the silicic eruptions were highly explosive. In addition, some Yemen ignimbrites from the upper bimodal phase are amphibole-bearing, indicating that magmas had minimum water contents of 4% (Merzbacher and Eggler 1984) (Table 1).

The observed differences in eruption volumes and lateral distribution between Yemen on-land tuffs and ignimbrites and Paraná-Etendeka rheoignimbrites are striking. Paraná rheoignimbrites are as much as an order of magnitude larger for on-land deposits. Distal airfall deposits have yet to be identified for Paraná-Etendeka rheoignimbrites, however, in contrast to distal airfall deposits correlated to several individual Yemen ignimbrites (Table 4; Ukstins Peate et al. 2003b; Touchard et al. 2003b). If the distal air fall tuffs associated with Yemen ignimbrites are included, maximum volume estimates for the two provinces become similar, but known areal distribution is more than an order of magnitude larger for Afro-Arabian tuffs than for Paraná-Etendeka rheoignimbrites (10^6 km^2 versus 4×10^4 km^2: Milner et al. 1995). It should be noted that there may be distal ash layers that correlate to the Paraná-Etendeka rheoignimbrites, but they have yet to be identified (e.g. Peate 1997). This suggests that the Paraná-Etendeka silicic eruptions may have had eruptive volumes 2 to 3 times as large as current estimates if distal tuffs are identified.

The differences in eruption volume and pyroclastic distribution between the Paraná-Etendeka and Afro-Arabian provinces reflect the inherent differences in eruption and dispersal mechanisms, which depend on magma rheology and, in turn, on eruption temperatures, magma composition and volatile content (e.g. Kirstein et al. 2001). In Yemen, lower eruption temperatures, coupled with potentially higher volatile contents, may have promoted more explosive eruptions, producing thinner on-land ash flow deposits but enhancing air fall tuff distribution through high eruption columns. Mechanisms for silicic magma generation such as crustal melting vs. extreme fractional crystallization of basalt (e.g. Garland et al. 1995; Baker et al. 1996b; Ewart et al. 1998; Kirstein et al. 2001; Ayalew et al. 2002) may also have had a significant role in governing the different eruptive styles through controls on magma volume, temperature and volatile content. These issues are complex, and will be addressed in a separate paper on the petrogenesis of the Yemen silicic magmas.

Summary

1. We have presented the first detailed description of Afro-Arabian silicic pyroclastic volcanic rocks in Yemen, characterizing volcanism as dominated by explosive ash fall and flow units and a caldera collapse breccia which preserve primary pyroclastic textures such as fiammé, basal vitrophyres and accretionary lapilli.
2. We identify three phases of flood volcanism: (i) effusive eruption of the main basaltic flood lavas, with minor intercalated distal silicic ash fall tuffs and the oldest ignimbrite known in the province (from 30.3 to 29.7 Ma, with a duration of 0.57 ± 0.30 Ma), (ii) the main stage of silicic pyroclastic eruptions, dominated by ash fall tuffs and ignimbrites, and (from 29.7 to 29.5 Ma, with a duration of 0.25 ± 0.23 Ma), (iii) an upper bimodal volcanic phase with intercalated basaltic and silicic lavas, ash fall tuffs and ignimbrites (from 29.5 to ~27.7 Ma, with a duration of 1.81 ± 0.25 Ma). Eight large volume silicic eruptive units are identified in northern Yemen, some of which have been geochemically correlated across the conjugate rifted margins of the Red Sea to Ethiopia and to Indian Ocean drill cores containing distal tephra layers.

3. The main silicic eruption units have preserved on-land volumes of up to ~1,000 km^3. The correlated distal tuff deposits indicate ash fall-out over areas $>1\times10^7$ km^2, and the minimum volume for a single eruption (Sam Ignimbrite) is ~3,100 km^3 (DRE) which is equivalent to a total erupted mass of 7.4×10^{15} kg.
4. Changes in eruption volumes and styles of silicic volcanism from the main silicic phase to the upper bimodal phase, including the transition from large-volume, highly explosive pyroclastic eruptions to small-volume, localized ignimbrites, tuffs and lavas, may reflect the initiation of continental rifting and concomitant crustal thinning during break-up at ca. 29.5 Ma, which prevented large-volume crustal magma chambers from being established.
5. Eruptive volume estimates for on-land rheoignimbrites from the Paraná-Etendeka province are an order of magnitude larger than for Afro-Arabian ignimbrites, but Afro-Arabian distal tephras indicate near-global ash dispersal and that silicic explosive eruptions from Yemen were globally significant. Yemen silicic eruptive units represent relatively lower temperature, highly explosive eruptions that produced welded ignimbrites and voluminous ash fall tuffs, in contrast to the Paraná-Etendeka silicic eruptions which were high-temperature and probably less explosive.

Acknowledgements We would like to thank David Pyle, Scott Bryan, Olivier Bachmann, Dougal Jerram and Julie Donnelly-Nolan for thorough comments on a previous version of this manuscript. Jon Davidson and Hillary Downes provided helpful comments when examining the Ph.D. thesis this work is based upon. I.U.P. would like to acknowledge support from a joint Ph.D. fellowship funded by the Danish Lithosphere Centre and Royal Holloway, University of London. The Danish Lithosphere Centre was supported by the Danish National Research Council. P.R.R. acknowledges support from NSF grant EAR-9909517. We acknowledge the field assistance of Tom Hagensen in Yemen. We would also like to thank Tod Waight for his assistance in the DLC MC-ICP-MS laboratory.

References

Al-Subbary AA (1995) The sedimentology and stratigraphy of the Cretaceous-early Tertiary Tawilah group, western Yemen. Ph.D. thesis, Royal Holloway University of London, pp 1–184

Axen GJ, Taylor WJ, Bartley JM (1993) Space-time patterns and tectonic controls of Tertiary extension and magmatism in the Great Basin of the western United States. GSA Bull 105:56–76

Ayalew D, Barbery P, Marty B, Reisberg L, Yirgu G, Pik R (2002) Source, genesis, and timing of giant ignimbrite deposits associated with Ethiopian continental flood basalts. Geochim Cosmochim Acta 66:1429–1448

Bachmann O, Dungan MA, Lipman PW (2002) The Fish Canyon magma body, San Juan volcanic field, Colorado: Rejuvenation and eruption of an upper crustal batholith. J Petrol 43:1469–1503

Baker J (1996) Stratigraphy, geochronology and geochemistry of Cenozoic volcanism in western Yemen. Ph.D. thesis, Royal Holloway University of London 386 pp

Baker JA, Snee L, Menzies M (1996a) A brief Oligocene period of flood volcanism: implications for the duration and rate of continental flood volcanism at the Afro-Arabian triple junction. Earth Planet Sci Lett 138:39–55

Baker JA, Thirlwall MF, Menzies MA (1996b) Sr-Nd-Pb isotopic and trace element evidence for crustal contamination of plume-derived flood basalts: Oligocene flood volcanism in western Yemen. Geochim Cosmochim Acta 60:2559–2581

Baker JA, Macpherson CG, Menzies MA, Thirlwall MF, Al-Kadasi M, Mattey DP (2000) Resolving crust and mantle contributions to continental flood volcanism, Yemen: constraints from mineral oxygen isotope data. J Petrol 41:1805–1820

Baker JA, Waight TE, Ulfbeck D (2002) Rapid and highly reproducible analysis of rare earth elements by multiple collector inductively coupled plasma mass spectrometry. Geochim Cosmochim Acta 66:3635–3646

Baker JA, Peate DW, Waight TE, Meyzen C (2004) Pb isotopic analysis of standards and samples using a^{207}Pb-^{204}Pb double spike and thallium to correct for mass bias with a double focusing MC-ICP-MS. Chem Geol 211:275–303

Beane JE, Turner CA, Hooper PR, Subbarao KV, Walsh JN (1986) Stratigraphy, composition and form of the Deccan basalts, western Ghats, India. Bull Volcanol 48:61–83

Berhe SM, Desta B, Nicoletti M, Teferra M (1987) Geology, geochronology and geodynamic implications of the Cenozoic magmatic province in W and SE Ethiopia. J Geol Soc London 144:213–226

Best MG, Christiansen EH (1997) Origin of broken phenocrysts in ash-flow tuffs. GSA Bull 109:63–73

Bonadonna C, Ernst GGJ, Sparks RSJ (1998) Thickness variations and volume estimates of tephra fall deposits: the importance of particle Reynolds number. J Volcanol Geotherm Res 81:173–187

Branney MJ, Kokelaar P (1994) Volcanotectonic faulting, soft-state deformation, and rheomorphism of tuffs during development of a piecemeal caldera, English Lake District. J Geol Soc London 106:507–530

Branney MJ, Kokelaar P (2002) Pyroclastic density currents and the sedimentation of ignimbrites. Geol Soc London Memoir 27:1–143

Bryan SE, Ewart A, Stephens CJ, Parianos J, Downes PJ (2000) The Whitsunday volcanic province, central Queensland, Australia: lithological and stratigraphic investigations of a silicic-dominated large igneous province. J Volcanol Geotherm Res 99:55–78

Bryan SE, Riley TR, Jerram DA, Stephens CJ, Leat PT (2002) Silicic volcanism: an undervalued component of large igneous provinces and volcanic rifted margins. In: Menzies MA, Klemperer SL, Ebinger CJ, Baker J (eds) Volcanic rifted margins. GSA Special Paper, pp 97–118

Calder ES, Sparks RSJ, Gardeweg MC (2000) Erosion, transport and segregation of pumice and lithic clasts in pyroclastic flows inferred from ignimbrite at Lascar Volcano, Chile. J Volcanol Geotherm Res 104:201–235

Capaldi G, Manetti P, Piccardo GB (1983) Preliminary investigations on volcanism of the Sa'dah region (Yemen Arab Republic). Bull Volcanol 46:413–427

Chiesa S, LaVolpe L, Lirer L, Orsi G (1983) Geological and structural outline of the Yemen Plateau, Yemen Arab Republic. Neues Jahr Geol 11:641–656

Civetta L, LaVolpe L, Lirer L (1978) K-Ar ages of the Yemen plateau. J Volcanol Geotherm Res 4:307–314

Dadd KA (1998) Origin and significance of megabreccia blocks in the Silurian Goobarragandra Volcanics, southeastern New South Wales. Aus J Earth Sci 45:315–321

Davidson A, Rex DC (1980) Age of volcanism and rifting in southwestern Ethiopia. Nature 283:657–658

Davison I et al 13 others (1994) Geological evolution of the southeastern Red Sea rift margin, Republic of Yemen. GSA Bull 106:1474–1493

Drury SA, Kelley SP, Berhe SM, Collier R, Araha M (1994) Structures related to the Red Sea evolution in northern Eritrea. Tectonics 13:1371–1380

Elliot DH (2000) Stratigraphy of Jurassic pyroclastic rocks in the Transantarctic Mountains. J Afr Earth Sci 31:77–88

Ewart A, Milner SC, Armstrong RA, Duncan AR (1998) Etendeka volcanism of the Goboboseb mountains and Messum igneous complex, Namibia. Part II: voluminous quartz latite volcanism of the Awahab magma system. J Petrol 39:227–253

Freundt A, Wilson CJN, Carey SN (2000) Ignimbrites and block-and-ash flow deposits. In: Sigurdsson H (ed) Encyclopedia of Volcanoes, pp 581–599

Gardner JE, Thomas RME, Jaupart C, Tait S (1996) Fragmentation of magma during Plinian volcanic eruptions. Bull Volcanol 58:144–162

Garland F, Hawkesworth CJ, Mantovani MSM (1995) Description and petrogenesis of the Paraná rhyolites, southern Brazil. J Petrol 36:1193–1127

Geoffroy LP, Huchon P, Khanbari K (1998) Did Tertiary granites intrude neck zones of a stretched continental crust? Terra Nova 10:196–200

Hargrove HR, Sheridan MF (1984) Welded tuffs deformed into megarheomorphic folds during collapse of the McDermitt Caldera, Nevada-Oregon. J Geophys Res 89:8629–8638

Heyckendorf K, Jung D (1991) The Neogene ash-flow caldera of A'ithayn: An eruptive centre upon the Trap Series in central North Yemen. Tectonophys 198:223–238

Hofmann C, Courtillot V, Féraud G, Yirgu E, Ketefo E, Pik R (1997) Timing of the Ethiopian flood basalt event and implications for plume birth and global change. Nature 389:838–841

Houghton BF, Wilson CJN, McWilliams MO, Lanphere MA, Weaver SD, Briggs RM, Pringle MS (1995) Chronology and dynamics of a large silicic magma system: Central Taupo Volccanic Zone, New Zealand. Geology 23:13–16

Jerram DA, Mountney N, Holzförster F, Stollhofen H (1999) Internal stratigraphic relationships in the Etendeka Group in the Huab Basin, NW Namibia: understanding the onset of flood volcanism. J Geodynamics 28:393–418

Jerram DA (2002) Volcanology and facies architecture of flood basalts. In: Menzies MA, Klemperer SL, Ebinger CJ, Baker JA (eds) Volcanic Rifted Margins, Geological Society of America, Special Paper 362:119–174

Kirstein LA, Hawkesworth CJ, Garland FG (2001) Felsic lavas or rheomorphic ignimbrites: Is there a chemical distinction? Contrib Mineral Petrol 142:309–322

Koyaguchi T, Tokuno M (1993) Origin of the giant eruption cloud of Pinatubo, June 15, 1991. J Volcanol Geotherm Res 55:85–96

Kruck W (1983) Geological map of the Yemen Arab Republic. Sheet Sana'a 1:250,000 Hannover Federal Inst. Geosci & Nat Res.

Kruck W, Schaffer U, Thiele J (1996) Explanatory notes on the Geological Map of the Republic of Yemen – western part – (former Yemen Arab Republic). Geol Jahrbuch B 87:3–104

Le Bas MJ, Le Maitre RW, Streckeisen A, Zanettin B (1986) A chemical classification of volcanic rocks based on the total alkali-silica diagram. J Petrol 27:745–750

Lipman PW (1976) Caldera-collapse breccias in the western San Juan Mountains, Colorado. GSA Bull 87:1397–1410

Manetti P, Capaldi G, Chiesa S, Civetta L, Conticelli S, Gasparon M, LaVolpe L, Orsi G (1991) Magmatism of the eastern Red Sea margin in the northern part of Yemen from Oligocene to present. Tectonophys 198:181–202

Mangan MT, Wright TL, Swanson DA, Byerly GR (1986) Regional correlation of Grande Ronde flows, Columbia River basalt group, Washington, Oregon and Idaho. Bull Geol Soc Am 97:1300–1318

Marsh JS, Ewart A, Duncan AR, Miller RM (2001) The Etendeka Igneous Province: magma types and their stratigraphic distribution with implications for the evolution of the Paraná-Etendeka flood basalt province. Bull Volcanol 62:464–486

McDougall I, Morton WH, Williams MAJ (1975) Age and denudation rate of Traps Series basalts at Blue Nile gorge, Ethiopia. Nature 254:207–209

Menzies MA, Gallagher K, Yelland A, Hurford A (1997) Volcanic and non-volcanic rifted margins of the Red Sea and Gulf of Aden: Crustal cooling and margin evolution in Yemen. Geochim Cosmochim Acta 61:2511–2527

Merzbacher C, Eggler DH (1984) A magmatic geohygrometer: application to Mount St. Helens and other dacitic magmas. Geology 12:587–590

Milner SC, Duncan AR, Ewart A (1992) Quartz latite rheoignimbrite flows of the Etendeka Formation, north western Namibia. Bull Volcanol 54:200–219

Milner SC, Duncan AR, Whittingham AM, Ewart A (1995) Trans-Atlantic correlation of eruptive sequences and individual silicic units within the Paraná-Etendeka igneous province. J Volcanol Geotherm Res 69:137–157

Mohr P (1983) Ethiopian flood basalt province. Nature 303:577–584

Mohr P (1991) Structure of Yemeni Miocene dike swarms, and emplacement of coeval granite plutons. Tectonophysics 198:203–221

Mohr P, Zanettin B (1988) The Ethiopian flood basalt province. In: MacDougall JD (ed) Continental flood basalts, Kluwer, Dordrecht, pp 63–110

Moore CL (1991) The distal terrestrial record of explosive rhyolitic volcanism: an example from Auckland, New Zealand. Sed Geol 74:25–38

Peate DW (1997) The Paraná-Etendeka province. In: Mahoney JJ, Coffin MF (eds) Large igneous provinces: continental, oceanic and planetary flood volcanism. AGU Geophysical Monograph 100:217–245

Peate DW, Hawkesworth CJ, Mantovani MSM, Shukowsky W (1990) Mantle plumes and flood-basalt stratigraphy in the Paraná, South America. Geology 18:1223–1226

Peate DW, Hawkesworth CJ, Mantovani MSM (1992) Chemical stratigraphy of the Paraná lavas (South America): classification of magma types and their spatial distribution. Bull Volcanol 55:119–139

Pik R, Deniel C, Coulon C, Yirgu G, Hofmann C, Ayalew D (1998) The northwestern Ethiopian plateau flood basalts: Classification and spatial distribution of magma types. J Volcanol Geoth Res 81:91–111

Pyle DM (1989) The thickness, volume and grainsize of tephra fall deposits. Bull Volcanol 51:1–15

Pyle DM (1995) Assessment of the minimum volume of tephra fall deposits. J Volcanol Geotherm Res 69:379–382

Pyle DM (1999) Widely dispersed Quaternary tephra in Africa. Global and Planetary Change 21:95–112

Renne PR, Swisher CS, Deino AL, Karner DB, Owens TL, DePaolo DJ (1998) Intercalibration of standards, absolute ages and uncertainties in $^{40}Ar/^{39}Ar$ dating. Chem Geol 145:117–152

Riisager P, Baker JA, Ukstins IA (2001) Paleomagnetic and anisotropy of magnetic susceptibility studies of Oligocene flood volcanism in Yemen. EOS (AGU Transactions) 82:GP11A–0195

Riisager P, Knight K, Baker JA, Ukstins Peate I, Al-Kadasi M, Al-Subbary A, Renne PR (in press) Paleomagnetism and $^{40}Ar/^{39}Ar$ Geochronology of Yemenite Oligocene volcanics: implications for timing and duration of Afro-arabian traps and geometry of the Oligocene paleomagnetic field. Earth and Planet Sci Lett.

Rochette P, Tamrat E, Féraud G, Pik R, Courtillot V, Ketefo E, Coulon C, Hofmann C, Vandamme D, Yirgu G (1998) Magnetostratigraphy and timing of the Oligocene Ethiopian traps. Earth Planet Sci Lett 164:497–510

Rose WI, Chesner CA (1987) The dispersal of ash in the great Toba eruption, 75 ka. Geology 15:913–917

Ross PS, Ukstins Peate IU, McClintock MK, Xu YG, Skilling IP, White JDL, Houghton BF (2005) Mafic volcaniclastic deposits in flood basalt provinces: a review. J. Volcanol. Geotherm Res, in press.

Self S (1992) Krakatau revisited: the course of events and interpretation of the 1883 eruption. GeoJournal 28:109–121

Smith RL (1960) Zones and zonal variations in welded ash flows. US Geological Survey Professional Paper, 354-F

Sparks RSJ, Walker GPL (1977) The significance of vitric-enriched air-fall ashes associated with crystal-enriched ignimbrites. J Volcanol Geotherm Res 2:329–341

Thompson MD (1985) Evidence for a Late Precambrian caldera in Boston, Massachusetts. Geology 13:641–643

Tommasini S, Poli G, Manetti P, Conticelli S (1994) Oligo-Miocene A-type granites and granophyres from Yemen; isotopic and trace-element constraints bearing on their genesis. Europ J Mineral 6:571–590

Touchard Y, Rochette P, Aubry MP, Michard A (2003a) High-resolution magnetostratigraphic and biostratigraphic study of Ethiopian traps-related products in Oligocene sediments from the Indian Ocean. Earth Planet Sci Lett 206:493–508

Touchard Y, Rochette P, Hamelin B, Michard A (2003b) Long distance transport of glass shards from Ethiopian traps megaplinian eruptions. IUGG General Assembly A.204

Ukstins IA, Renne PR, Wolfenden E, Baker J, Ayalew D, Menzies M (2002) Matching conjugate rifted margins: $^{40}Ar/^{39}Ar$ chrono-stratigraphy of pre- and syn-rift bimodal flood volcanism in Ethiopia and Yemen. Earth Planet Sci Lett 198:289–306

Ukstins Peate IA (2003) Volcanostratigraphy, geochronology and geochemistry of silicic volcanism in the Afro-Arabian flood volcanic province (Yemen and Ethiopia). Ph.D. thesis, Royal Holloway University of London 412 pp

Ukstins Peate IA, Larsen M, Lesher CE (2003a) The transition from sedimentation to flood volcanism in the Kangerlussuaq Basin, East Greenland: basaltic pyroclastic volcanism during initial Paleogene continental break-up. J Geol Soc London 160:759–772

Ukstins Peate IA, Baker JA, Kent AJR, Al-Kadasi M, Al-Subbary AK, Ayalew D, Menzies M (2003b) Correlation of Indian Ocean tephra to individual silicic eruptions from the Oligocene Afro-Arabian flood volcanic province. Earth Planet Sci Lett 211:311–327

WoldeGabriel G, Aronson JL, Walter RC (1990) Geology, geochronology, and rift basin development in the central sector of the Main Ethiopian Rift. Geol Soc Am Bull 102:439–458

Wolff JA (1985) Zonation, mixing and eruption of silica-undersaturated alkaline magma; a case study from Tenerife, Canary Islands. Geol Mag 122:623–640

Woods AW, Self S (1992) Thermal disequilibrium at the top of volcanic clouds and its effect on estimates of the column height. Nature 355:628–630

Woods AW, Wohletz K (1991) Dimensions and dynamics of co-ignimbrite eruption columns. Nature 350:225–227